Non-canonical activation of IRE1α during *Candida albicans* infection enhances macrophage fungicidal activity

Michael J. McFadden [1], Mack B. Reynolds [1], Britton C Michmerhuizen [1,a], Faith M. Anderson [1], Mary X.D. O'Riordan[†] [1], Teresa R. O'Meara[†] [1]

Affiliations:

[1] Department of Microbiology and Immunology, University of Michigan, Ann Arbor, MI 48109, USA.

Michael J. McFadden; mcfaddmj@umich.edu, Mack B. Reynolds; mbreyn@umich.edu, Britton C Michmerhuizen; michmer8@msu.edu, Faith M. Anderson; faithma@umich.edu, Teresa R. O'Meara; tromeara@umich.edu, Mary X.D. O'Riordan; oriordan@umich.edu

[a] Current affiliation: College of Human Medicine, Michigan State University, Grand Rapids, MI 49503, USA.

[†] Corresponding author

Correspondence to tromeara@umich.edu or oriordan@umich.edu

Abstract

Infection by intracellular pathogens can trigger activation of the IRE1α branch of the unfolded protein response (UPR), which then modulates innate immunity and infection outcomes during bacterial or viral infection. However, the mechanisms by which infection activates IRE1α have not been fully elucidated. While recognition of microbe-associated molecular patterns can activate IRE1α, it is unclear whether this depends on the canonical role of IRE1α in detecting misfolded proteins. Here, we report that *Candida albicans* infection of macrophages results in IRE1α activation through C-type lectin receptor signaling, reinforcing a role for IRE1α as a central regulator of host responses to infection by a broad range of pathogens. However, IRE1α activation was not preceded by protein misfolding in response to either *C. albicans* infection or lipopolysaccharide treatment, implicating a non-canonical mode of IRE1α activation after recognition of microbial patterns. Investigation of the phenotypic consequences of IRE1α activation in macrophage antimicrobial responses revealed that IRE1α activity enhances the fungicidal activity of macrophages. Macrophages lacking IRE1α activity displayed inefficient phagolysosomal fusion, enabling *C. albicans* to evade fungal killing and escape the phagosome. Together, these data provide mechanistic insight for the non-canonical activation of IRE1α during infection, and reveal central roles for IRE1α in macrophage antifungal responses.

Introduction

Intracellular infection by diverse pathogens triggers cell stress programs that influence infection outcomes through regulation of innate immunity, cellular metabolism and homeostasis, and cell differentiation or cell death pathways[1,2]. For example, infection with diverse pathogens can trigger activation of the unfolded protein response (UPR), whose three branches (IRE1α, PERK, and ATF6) have broad consequences for host antimicrobial defenses[3,4]. Canonically, accumulation of misfolded proteins in the ER lumen triggers activation of the UPR[5]. As proteostasis is required for cellular function, UPR activation can restore cellular homeostasis by modulating gene expression to promote protein folding and expansion of the ER network. Alternatively, failure to overcome proteotoxic stress leads to cell death[5]. Therefore, initiation of the UPR during infection may be critical to circumvent the effects of pathogen virulence factors, or to support the production of secreted proteins such as cytokines[4,6]. Still, the utility and effects of UPR activation during infection are not fully understood and differ in response to individual pathogens, which may differentially exploit UPR activation for pathogenesis[7–14].

Generally, IRE1α activation is triggered by its assembly into small oligomers that allow its *trans*-autophosphorylation[15]. Autophosphorylation of IRE1α results in activation of its

endonuclease domain, allowing IRE1α to remove a short intronic sequence from the *Xbp1* transcript in a non-canonical mRNA splicing reaction, orthologous to the Ire1-*Hac1* splicing reaction that drives the UPR in yeast[16–18]. *Xbp1* splicing results in a frameshift within the open reading frame, allowing translation and protein synthesis of the transcription factor XBP1S, which promotes the transcription of genes involved in ER quality control[19]. Interestingly, the IRE1α branch of the UPR can be selectively triggered by infection or detection of microbe-associated molecular patterns (MAMPs) by pattern recognition receptors (PRRs), such as Toll-like receptors (TLRs)[6,20]. Previous reports suggested that protein misfolding-independent activation of IRE1α may occur following TLR stimulation, although this model has not been directly tested[6,20]. Overall, the mechanisms by which IRE1α activation occurs during infection and MAMP exposure are incompletely understood.

IRE1α has broad regulatory roles and consequences for infection and immunity. For example, the IRE1α-XBP1S axis can promote the expression of proinflammatory cytokines[6,21], modulate metabolic plasticity[22], and promote ER homeostasis[23] during infection. Additionally, IRE1α can facilitate intra-organelle communication for ER-mitochondria calcium signaling and promotion of reactive oxygen species (ROS) generation[11,12,24]. Importantly, through its regulatory effects on gene expression, metabolism, and redox balance, IRE1α can promote bacterial killing or inflammasome activation in phagocytic cells[9,11]. Despite these known roles of IRE1α in bacterial and viral infection, mechanistic understanding of IRE1α activation during infection is lacking. Further, our understanding of the role of IRE1α during fungal infection is only beginning to emerge.

Given its many functions in host responses to infection, we sought to understand the role of IRE1α in macrophage interactions with *Candida albicans*. Interestingly, a recent report found that IRE1α can be activated in neutrophils upon *C. albicans* infection, and IRE1α activity contributes to the immunopathology of systemic *C. albicans* infection[13], revealing the importance of regulation of this pathway during infection. *C. albicans* is a common fungal member of the human mucosal microbiota and an opportunistic pathogen[25]. Phagocytic cells are an important early line of defense against systemic infection by *C. albicans*[26]. Neutrophils and macrophages can recognize and phagocytose *C. albicans* and eliminate infection through fungicidal activity or secretion of cytokines to orchestrate antifungal immunity[27–30]. Studies investigating *C. albicans* interactions with macrophages showed that *C. albicans* hyphal growth can allow it to escape the phagosome and kill macrophages through lytic or programmed cell death through pyroptosis[31–36]. However, the mechanisms by which macrophages contain and kill *C. albicans* are incompletely understood. Indeed, levels of microbicidal effectors, such as ROS, are not reliable predictors of

93 phagocyte fungicidal activity[37,38]. However, recent work reported that lysosome fusion with the
94 expanding *C. albicans*-containing phagosome is crucial to maintain phagosome integrity,
95 preventing phagosomal rupture and allowing fungicidal activity[38–41], thus suggesting that
96 phagosome maturation is a critical component of antifungal responses by macrophages.
97 Here, we report that IRE1α is activated in macrophages following infection by *C. albicans*.
98 Importantly, IRE1α activation was dependent on C-type lectin receptor (CLR) signaling, but did
99 not depend on detectable accumulation of misfolded proteins, suggesting a non-canonical
100 mechanism of activation. Additionally, we found IRE1α is dispensable for phagocytosis of *C.*
101 *albicans* by macrophages, but contributes to their fungicidal activity. Macrophages lacking IRE1α
102 activity failed to efficiently recruit lysosomes to the phagosome, which was followed by increased
103 phagosome rupture and more hyphal growth by *C. albicans*. These results reveal a role for IRE1α
104 in the fungicidal capacity of macrophages, advancing our understanding of the emerging role of
105 IRE1α in antifungal immunity.
106
107
108 **Results**
109 ***C. albicans* infection results in activation of macrophage IRE1α**
110 While the ER stress sensor IRE1α is activated in response to bacterial and viral infection,
111 its role and activation in response to fungal infections is only beginning to emerge. To determine
112 whether macrophage IRE1α is activated during *C. albicans* infection, we measured splicing of
113 *Xbp1* mRNA in immortalized bone marrow-derived macrophages (iBMDM) infected with *C.*
114 *albicans*, or treated with known IRE1α activating stimuli, bacterial lipopolysaccharide (LPS) or
115 thapsigargin, as positive controls. Using semi-quantitative RT-PCR analysis of *Xbp1* mRNA, we
116 observed that *C. albicans* infection induces *Xbp1* splicing in wild-type iBMDM (WT), albeit to a
117 lesser extent than the positive controls LPS and thapsigargin (Fig. 1A). *Xbp1* splicing did not occur
118 in response to any of the treatments in a clonal iBMDM cell line lacking exons 20 and 21 of IRE1α
119 ($IRE1^{\Delta R}$), which are required for its endonuclease activity[42] (Fig. 1A, 1B). Analysis of *Xbp1* splicing
120 by RT-qPCR following a timecourse of *C. albicans* infection showed induction of *Xbp1-S* at 4
121 hours post-infection (hpi) with *C. albicans* (Fig. 1C). As the SC5314 reference strain can be an
122 outlier in virulence and hyphal formation[25,43], we measured *Xbp1-S* induction following infection
123 with a selection of commensal *C. albicans* isolates previously isolated from healthy donors[25] and
124 demonstrated that all isolates resulted in comparable *Xbp1* splicing to the reference strain
125 SC5314 (Fig. 1D).

126 *Xbp1* splicing leads to translation of the transcription factor XBP1S to induce the
127 transcription of ER quality control responsive genes following unfolded protein stress. However,
128 while LPS and thapsigargin treatment led to accumulation of XBP1S by 4 hpi, infection with *C.*
129 *albicans* did not lead to induction of XBP1S protein expression at 4, 6, or 8 hours post-infection
130 (Fig. S1). Thus, IRE1α function during *C. albicans* infection of macrophages is likely independent
131 of the transcription factor XBP1S. Together, these results indicate that *C. albicans* infection results
132 in mild activation of IRE1α in macrophages.

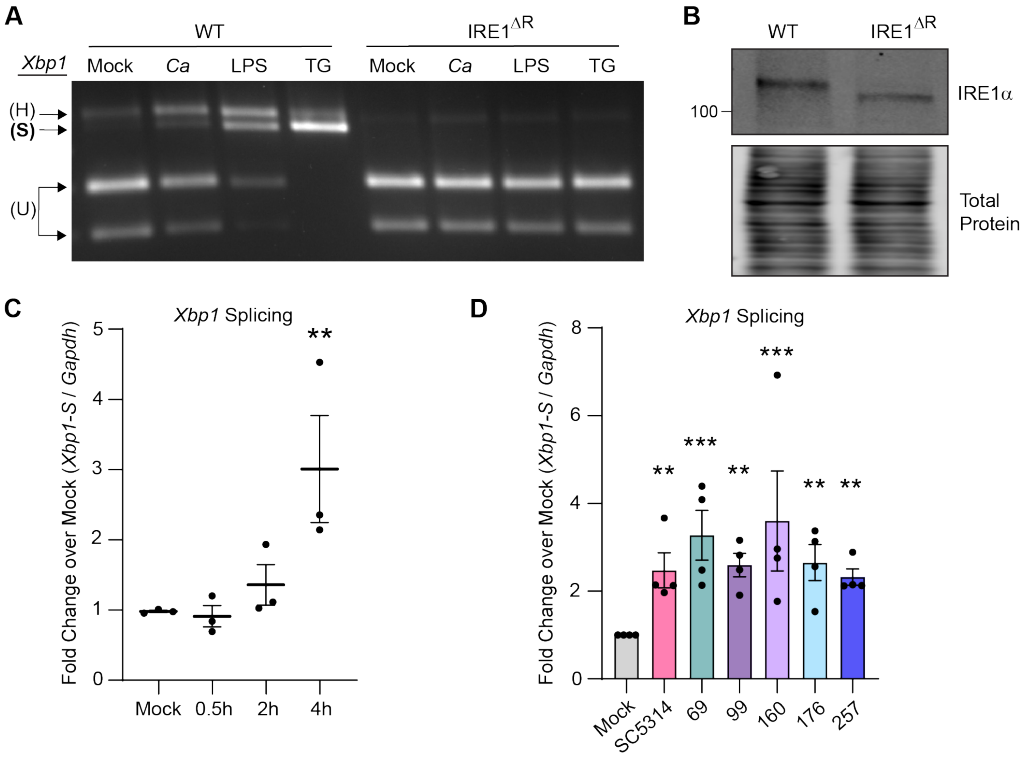

133

134 **Figure 1: *C. albicans* infection results in activation of macrophage IRE1α. (A)** iBMDM cell
135 lines (WT or IRE1$^{\Delta R}$) were infected with *C. albicans* (MOI=1), treated with LPS (100 ng/mL), or
136 thapsigargin (5 μM), or mock treated for 4 hours. *Xbp1* mRNA splicing was measured by semi-
137 quantitative RT-PCR amplification of the *Xbp1* transcript as a readout of IRE1α activity. **(B)**
138 Immunoblot analysis of lysates from WT or IRE1$^{\Delta R}$ iBMDM cell lines to confirm IRE1α truncation
139 in IRE1$^{\Delta R}$ cells resulting from removal of floxed exons 20 and 21. **(C)** Expression of the short
140 isoform of *Xbp1* was measured using RT-qPCR over a timecourse following *C. albicans* infection
141 of iBMDM (MOI=1). **(D)** Expression of the short isoform of *Xbp1* at 4 hours post-infection with
142 commensal *C. albicans* isolates as well as the lab strain SC5314 (MOI=1) was measured using
143 RT-qPCR. Data are representative of 3-4 individual experiments. Graphs show the mean ± SEM
144 of biological replicates. *$p < 0.05$, **$p < 0.01$, ***$p < 0.005$ by 2-way ANOVA of log-transformed
145 data with Sidak's multiple comparisons test (C and D).

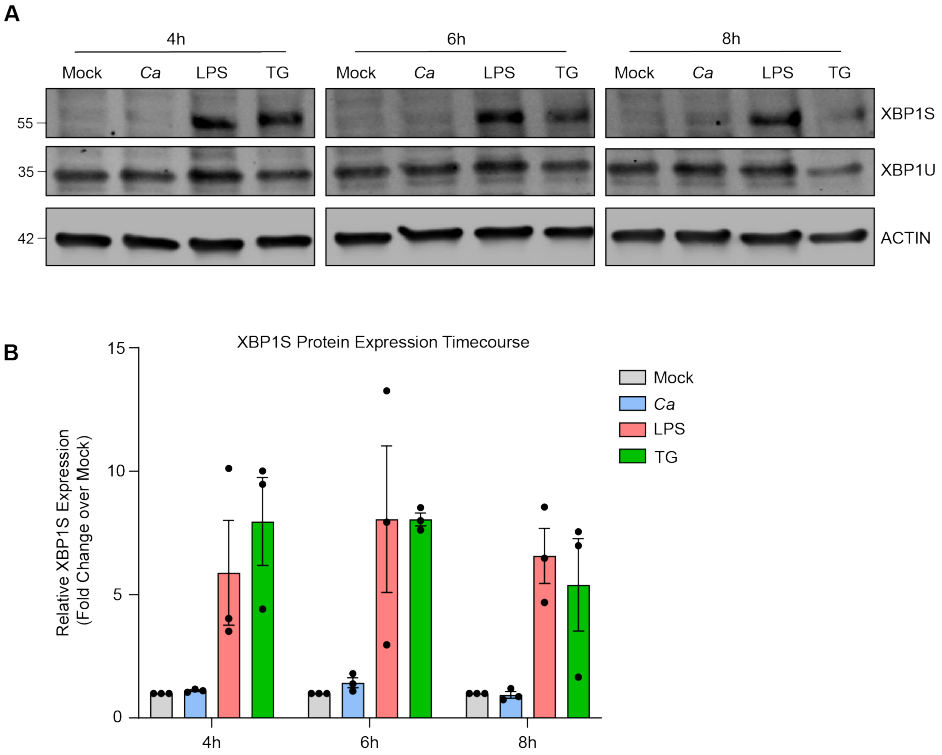

Figure S1: Related to Figure 1. (A) Immunoblot analysis of XBP1S and XBP1U expression from WT iBMDM lysates following infection with *C. albicans* (MOI=1), or treatment with positive controls LPS (100 ng/mL) or thapsigargin (5 uM). **(B)** Quantification of 3 independent experiments, as shown in (A).

C-type lectin receptor signaling drives TRAF6-independent IRE1α activation during *C. albicans* infection.

C-type lectin receptors, which detect components of the cell wall of *C. albicans*[28], are the major pattern recognition receptor for recognition of *C. albicans* in macrophages[44]. To determine whether C-type lectin receptor (CLR) signaling contributes to IRE1α activation during *C. albicans* infection, we measured *Xbp1* splicing in iBMDM lacking the CLR signaling adaptor protein CARD9 (CARD9 KO), compared to WT iBMDM. CARD9 was required for *Xbp1* splicing in response to *C. albicans*, but dispensable for *Xbp1* splicing in response to LPS, which activates a distinct signaling pathway through Toll-like receptor 4 (TLR4)[45,46] (Fig. 2A). These results suggest CLR signaling is required for IRE1α activation in response to *C. albicans*. Next, we addressed whether CLR agonism is sufficient to stimulate IRE1α activity by treating WT or IRE1$^{\Delta R}$ iBMDM with a Dectin-1 specific agonist, depleted Zymosan (d-Zymosan). We found that depleted Zymosan treatment

165 was sufficient to trigger IRE1α-dependent *Xbp1* splicing, demonstrating that CLR agonism
166 triggers IRE1α activity (Fig. 2B). Similar to results with *C. albicans* infection, *Xbp1* processing by
167 IRE1α was more strongly stimulated by LPS than by depleted Zymosan (Fig. 2B). Despite CLRs
168 being the major pattern recognition receptors for *C. albicans,* TLRs can also respond to fungal
169 cells[47]. To test whether TLR engagement is necessary for IRE1α activation in response to *C.*
170 *albicans*, we measured *Xbp1* splicing in BMDM lacking TLR2, TLR4, and TLR9 (TLR2/4/9 KO).
171 We observed a similar level of *Xbp1* splicing to WT iBMDM in response to *C. albicans* and
172 depleted Zymosan, although *Xbp1* splicing was ablated in response to LPS, as expected (Fig.
173 2C). Together, these results suggest CLR signaling is necessary and sufficient for IRE1α
174 activation in response to *C. albicans*.
175 TRAF6 is a crucial E3 ubiquitin ligase involved in innate immune signaling for both TLR
176 and CLR pathways[48,49]. This ubiquitin ligase can directly ubiquitinate IRE1α and facilitates the
177 ubiquitination and activation of IRE1α after LPS treatment[6,20]. Therefore, we tested whether
178 TRAF6 is involved in IRE1α activation in response to *C. albicans* infection. While knockout of
179 TRAF6 resulted in the expected decrease in *Xbp1* splicing in response to LPS, we observed that
180 *Xbp1* splicing in response to *C. albicans* infection was not affected by TRAF6 deletion (Fig. 2D).
181 Therefore, CLR-mediated IRE1α activation is TRAF6-independent. These data reveal that CLR
182 signaling through the adaptor protein Card9 triggers IRE1α activation independently of TLR
183 signaling or TRAF6, and suggests a distinct mechanism of IRE1α activation during *C. albicans*
184 infection.

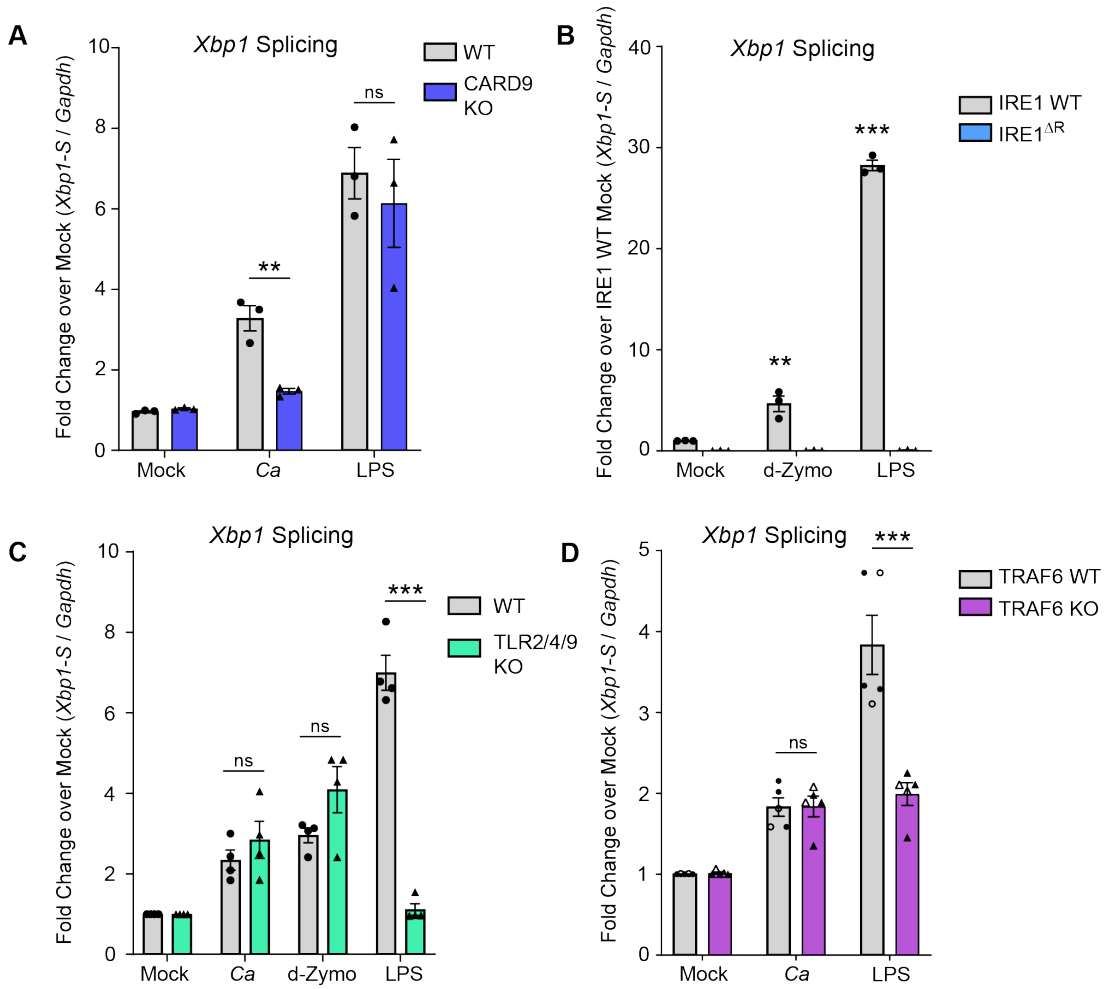

Figure 2: C-type lectin receptor signaling activates IRE1α during *C. albicans* infection. (A) Expression of the short isoform of *Xbp1* was measured using RT-qPCR following *C. albicans* infection (MOI=1) or LPS treatment (100 ng/mL) of WT or CARD9 KO iBMDM. **(B)** Expression of the short isoform of *Xbp1* was measured using RT-qPCR following *C. albicans* infection (MOI=1), depleted Zymosan treatment (d-Zymo; 100 ug/mL) to stimulate Dectin-1, or LPS treatment (100 ng/mL) of WT or IRE1$^{\Delta R}$ iBMDM. **(C)** Expression of the short isoform of *Xbp1* was measured using RT-qPCR following *C. albicans* infection (MOI=1), LPS treatment (100 ng/mL), or depleted Zymosan treatment (d-Zymosan; 100 ug/mL) of WT or TLR2/4/9 KO iBMDM. **(D)** Expression of the short isoform of *Xbp1* was measured using RT-qPCR following *C. albicans* infection or LPS treatment of two pairs of clonal iBMDM (WT or TRAF6 KO; MOI=1). Closed symbols are data from WT-1 and KO-1; open symbols are data from WT-2 and KO-2. Graphs show the mean ± SEM of biological replicates. *p < 0.05, **p < 0.01, ***p < 0.005 by 2-way ANOVA of log-transformed data with Sidak's multiple comparisons test. ns, not significant.

Supplemental Figure 2

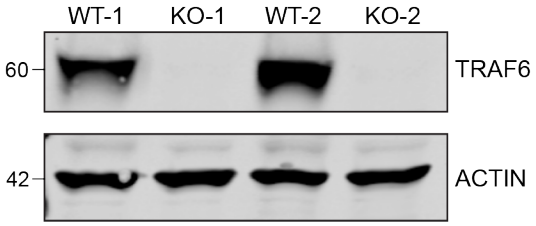

Figure S2: Confirmation of TRAF6 knockout. Immunoblotting validation of clonal TRAF6 WT controls (WT-1 and WT-2) and TRAF6 knockout iBMDM (KO-1 and KO-2).

PRR-mediated activation of IRE1α occurs independently of misfolded protein stress.

We hypothesized that innate immune receptor engagement and subsequent cytokine induction could activate IRE1α by overwhelming the protein folding capacity of the ER, leading to protein misfolding and thus IRE1α activation. To determine whether new gene synthesis is required for IRE1α activation during *C. albicans* infection, we inhibited transcription or translation during infection with *C. albicans* or during treatment with thapsigargin. Surprisingly, neither inhibition of transcription nor translation, using actinomycin D or cycloheximide treatment, respectively, inhibited *Xbp1* splicing during *C. albicans* infection (Fig. 3A-B). Translation inhibition using cycloheximide was sufficient to alleviate *Xbp1* splicing specifically in response to thapsigargin, likely by reducing the nascent protein folding burden (Fig. 3B). These data indicate that new gene synthesis does not contribute to IRE1α activation during *C. albicans* infection, and presented the intriguing possibility that infection does not induce unfolded proteins. Indeed, this possibility has been suggested for TLR-driven IRE1α activation, but was not directly tested[6,20]. To specifically test this, we measured whether misfolded proteins accumulate to drive IRE1α activation during PRR-mediated activation of IRE1α by either *C. albicans* infection or LPS treatment. Thioflavin T (ThT) is widely used to detect protein misfolding, as it exhibits increased fluorescence in the presence of misfolded proteins[50]. While ThT intensity showed an expected increase at 2 hours-post thapsigargin treatment, neither *C. albicans* infection nor LPS treatment increased ThT intensity over mock treatment (Fig. 3C-D). Further, neither *C. albicans* infection nor LPS treatment led to increased ThT intensity at 4 hpi, suggesting IRE1α activation occurs without accumulation of misfolded proteins during these responses (Fig. 3E). Even at 8 hpi, *C. albicans* infection did not induce protein misfolding (Fig. 3F). While LPS treatment did lead to increased protein misfolding at 8 hours post-treatment (Fig. 3F), this occurred after the robust IRE1α activation observed at 4 hours post-treatment (Fig. 1A). Together, these data suggest that

228 while protein misfolding can occur in response to microbial patterns, it is not needed to trigger
229 IRE1α activation during innate immune responses.
230
231

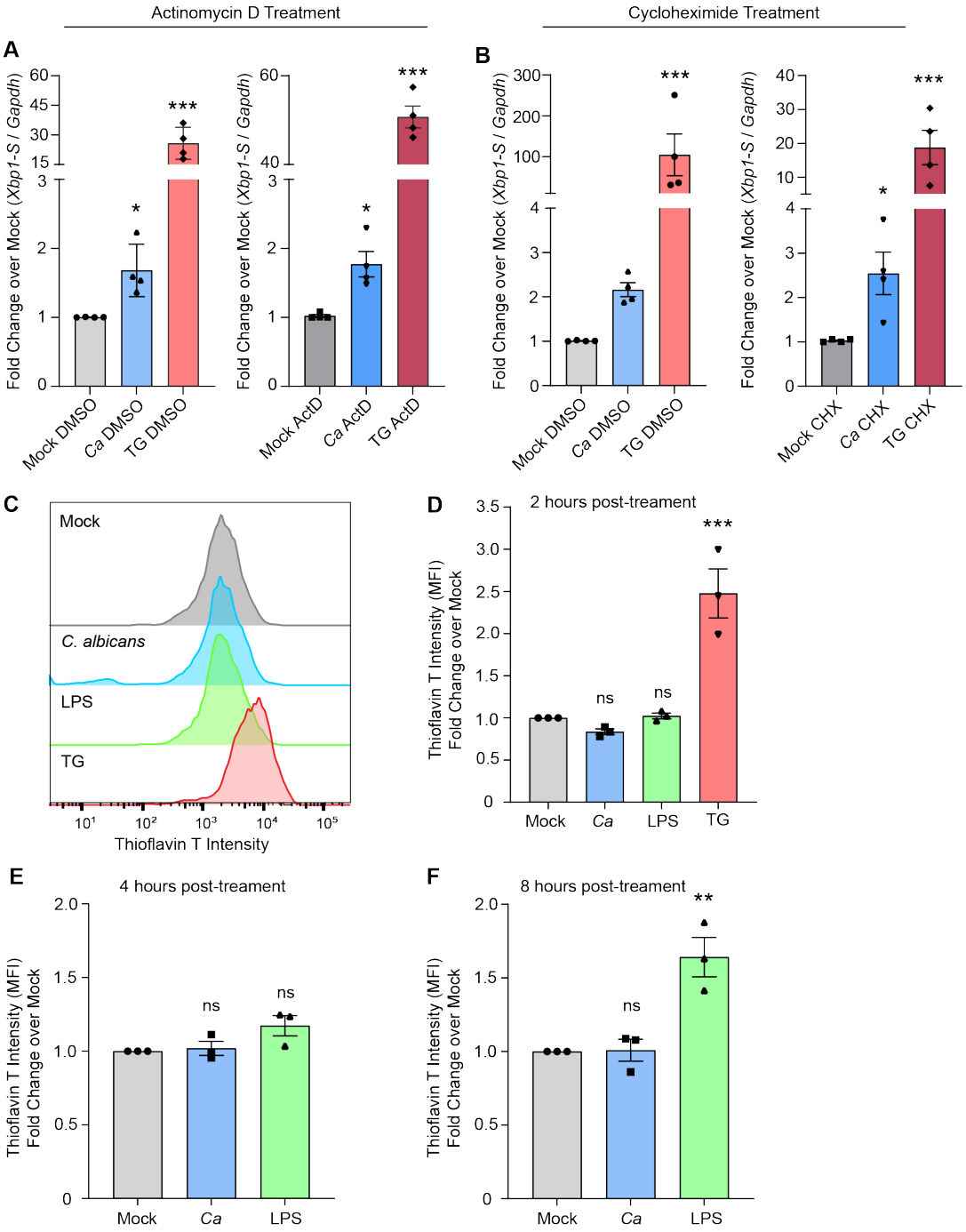

232
233 **Figure 3: PRR-mediated activation of IRE1α occurs independently of misfolded protein**
234 **stress. (A-B)** Expression of the short isoform of *Xbp1* was measured using RT-qPCR following

235 *C. albicans* infection (MOI=1) of iBMDM or treatment with thapsigargin (TG; 5 μM) as a control,
236 compared to Mock treatment. Actinomycin D (ActD; 20 μM) was used to inhibit new transcription
237 during treatments (A), and cycloheximide (CHX; 10 μM) was used to inhibit translation during
238 treatments (B), and relative fold changes were measured over matched mock samples. **(C)**
239 Representative graphs showing fluorescence intensity of Thioflavin T (ThT) measured by flow
240 cytometry to quantify protein misfolding in iBMDM following infection by *C. albicans* (MOI=1), or
241 treatment with LPS (100 ng/mL) or thapsigargin (TG; 5 μM) as a positive control. **(D-F)**
242 Quantification of ThT fluorescence intensity at 2 hours (D), 4 hours (E), or 8 hours post-indicated
243 treatment, shown as fold change over mock. Graphs show the mean ± SEM of biological
244 replicates. *$p < 0.05$, **$p < 0.01$, ***$p < 0.005$ by 2-way ANOVA with Sidak's multiple comparisons
245 test of log-transformed data (A, B) or one-way ANOVA with Tukey's multiple comparisons test (D-
246 F).
247
248 **IRE1α activity suppresses the expression of a subset of interferon-stimulated genes.**
249 To better understand how IRE1α activity contributes to macrophage responses to
250 infection, we investigated its impact on gene expression during *C. albicans* infection or mock
251 treatment using RNA sequencing. Despite not observing robust XBP1S induction during *C.*
252 *albicans* infection (Fig. S1), we reasoned that IRE1α activity could modulate gene expression by
253 XBP1S-independent mechanisms. For example, the RNase activity of IRE1α can cleave other
254 transcripts or microRNAs in a process known as regulated IRE1-dependent decay (RIDD)[51–53].
255 Additionally, IRE1α interacts with ER-localized RNA species under homeostatic or ER stress
256 conditions[54], therefore IRE1α may have broad consequences in gene expression regulation. As
257 expected, we found many differentially regulated genes in IRE1$^{\Delta R}$ macrophages during *C.*
258 *albicans* infection (Table S1.1) compared with WT macrophages at 4 hpi. Importantly, the IRE1$^{\Delta R}$
259 macrophages had broadly similar expression of ER stress-related genes as WT control
260 macrophages, suggesting that lack of IRE1 does not result in chronic ER stress during infection
261 (Fig. 4A). Interestingly, IRE1$^{\Delta R}$ macrophages had increased expression of interferon- and
262 infection-responsive genes, which was observed after mock treatment and exacerbated by *C.*
263 *albicans* infection (Fig. 4B; Table S1.2, S2.2). Analysis of 84 "core" ISGs[55], showed that IRE1$^{\Delta R}$
264 macrophages have basally increased expression of a specific subset of ISGs, and that this
265 difference is increased further during *C. albicans* infection (Fig. 4C, D).
266 Increased expression of proinflammatory gene expression observed in IRE1$^{\Delta R}$
267 macrophages in response to *C. albicans* infection was supported by ELISA analysis of
268 proinflammatory cytokines in supernatants of cultured cells. We observed that IL-1β and TNF

269 secretion were increased in IRE1$^{\Delta R}$ macrophages compared with IRE1 WT cells (Fig. 5A-C). As
270 an orthogonal method to test for the impact of IRE1α on cytokine responses, we used a chemical
271 inhibitor of IRE1α endonuclease activity, 4μ8C. Chemical probes provide an opportunity for fine-
272 grained dose and temporal control over the perturbation, and previous work using 4μ8C resulted
273 in a decrease in inflammatory cytokine outputs by macrophages in response to multiple
274 stimuli[20,56]. However, when we examined the effects of 4μ8C, we saw that this treatment
275 suppressed cytokine secretion in both WT and IRE1$^{\Delta R}$ macrophages, suggesting that it has off-
276 target effects that would account for its immunosuppressive activity (Fig. 5A-C). Indeed, previous
277 research showed that 4μ8C has potent cellular antioxidant activity[57]; this may explain the effects
278 on proinflammatory gene expression or ER stress[58]. These results highlight the importance of
279 cautious interpretation of the effect of 4μ8C treatment during infection.
280
281
282

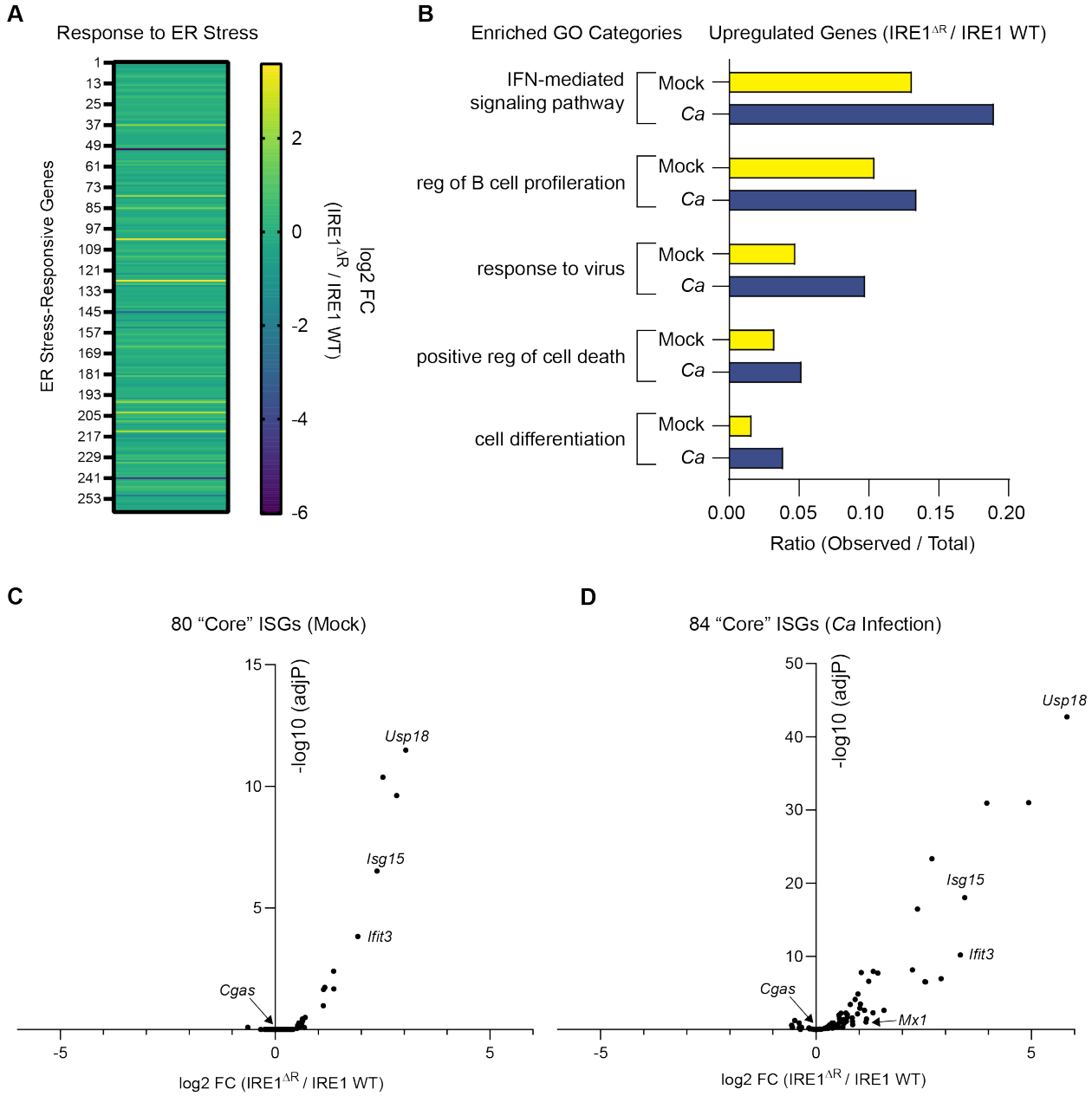

Figure 4: IRE1α suppresses interferon-stimulated gene transcription during *C. albicans* infection. (A) Heatmap differential gene expression in IRE1$^{\Delta R}$ iBMDM of genes in the GO category "Response to ER stress". **(B)** Gene ontology analysis of upregulated transcripts in IRE1$^{\Delta R}$ iBMDM (adjP<0.01, fold-change >2; n=615) reveals enrichment of interferon-stimulated genes. **(C-D)** Volcano plot of differential expression of "core" interferon-stimulated genes[55] in IRE1$^{\Delta R}$ iBMDM compared to IRE1 WT iBMDM during mock treatment (C) or *C. albicans* infection (MOI=1) (D).

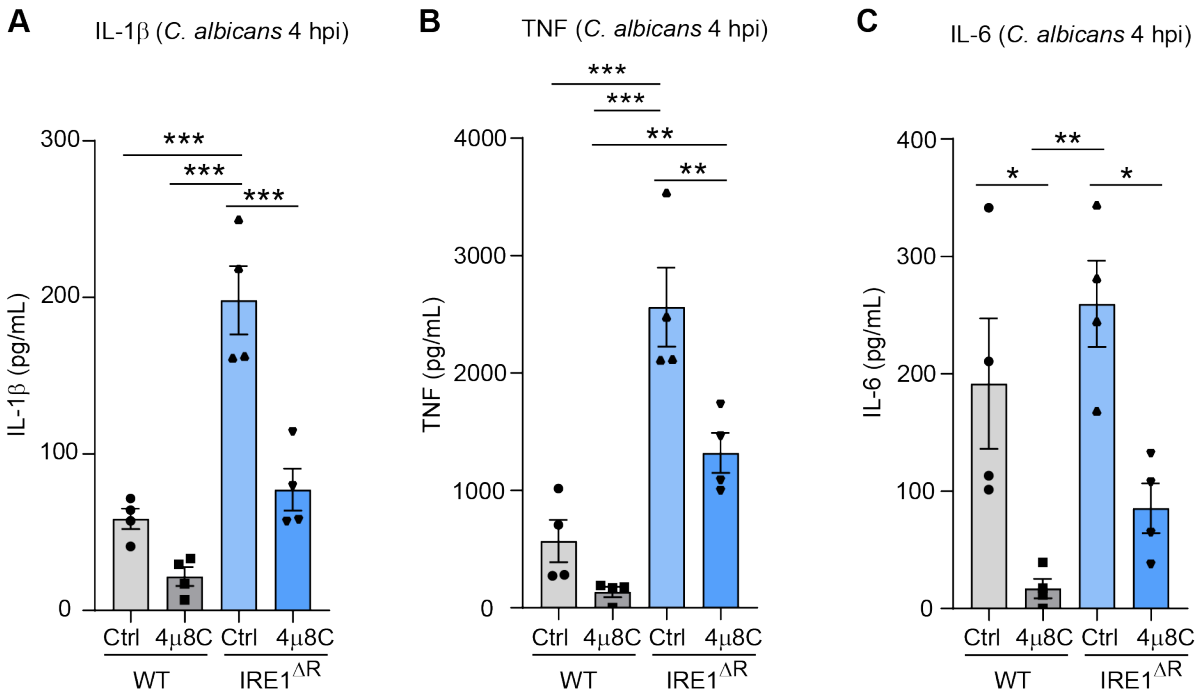

Figure 5: IRE1α suppresses early proinflammatory cytokine secretion during *C. albicans* infection. (A-C) Expression of proinflammatory cytokines (IL-1β (A), TNF (B), and IL-6 (C)) were measured by ELISA following 3 h of LPS priming and 5 h of *C. albicans* infection (MOI=1) in IRE1 WT and IRE1$^{\Delta R}$ iBMDM. Graphs show the mean ± SEM of 3 biological replicates. *$p < 0.05$, **$p < 0.01$, *** $p < 0.001$, by one-way ANOVA with Tukey's multiple comparisons test.

IRE1α contributes to fungal containment in the macrophage phagosome. Given the broad roles of IRE1α in macrophage antimicrobial functions[6,9,11], we next assessed the role of IRE1α in macrophage antifungal capacity with consideration of differential gene expression in IRE1$^{\Delta R}$ macrophages. Interestingly, gene ontology analysis of downregulated genes in IRE1$^{\Delta R}$ macrophages revealed that endocytosis and calcium signaling were enriched among these downregulated genes (Table S1.3). Therefore, we reasoned that endosomal maturation may be altered. Further, IFN-γ has previously been shown to alter phagosome maturation and downregulate the degradative capacity of the phagosome, perhaps to promote antigen presentation [59–61]. These findings are consistent with our observation that the expression of many interferon-responsive transcripts was increased in IRE1$^{\Delta R}$ macrophages (Fig. 4). Importantly, lysosome fusion with the expanding *C. albicans* containing phagosome is crucial for maintenance of the phagosomal membrane, which is needed to enable fungal killing [38,39]. To determine the role of IRE1α in the endocytic pathway during *C. albicans* infection, we first tested the ability of IRE1 WT and IRE1$^{\Delta R}$ macrophages to ingest *C. albicans* through phagocytosis. Interestingly, IRE1$^{\Delta R}$

313 macrophages showed increased efficiency of *C. albicans* phagocytosis (Fig. 6A-B). We then
314 tested whether IRE1$^{\Delta R}$ macrophages showed impaired phagolysosomal fusion during *C. albicans*
315 infection by measuring recruitment of the lysosomal protein LAMP1 to the phagosome containing
316 *C. albicans* (Fig. 6C-D). IRE1 WT macrophages recruited LAMP1 to the phagosome by 2 hpi, but
317 IRE1$^{\Delta R}$ macrophages infected with *C. albicans* failed to efficiently recruit LAMP1 to the
318 phagosome (Fig. 6C-D). However, overall lysosome biogenesis did not appear to be impaired in
319 IRE1$^{\Delta R}$ macrophages, as labeling acidic cellular compartments with LysoSensor Blue/Yellow dye
320 showed IRE1$^{\Delta R}$ macrophages had similar acidity as IRE1 WT macrophages, and *C. albicans*
321 infection or ammonium chloride treatment led to the expected alkalinization of both cell lines [41,62–
322 64] (Fig. 6E). These data suggest that IRE1α activity is specifically required for efficient
323 phagolysosomal fusion during *C. albicans* infection.

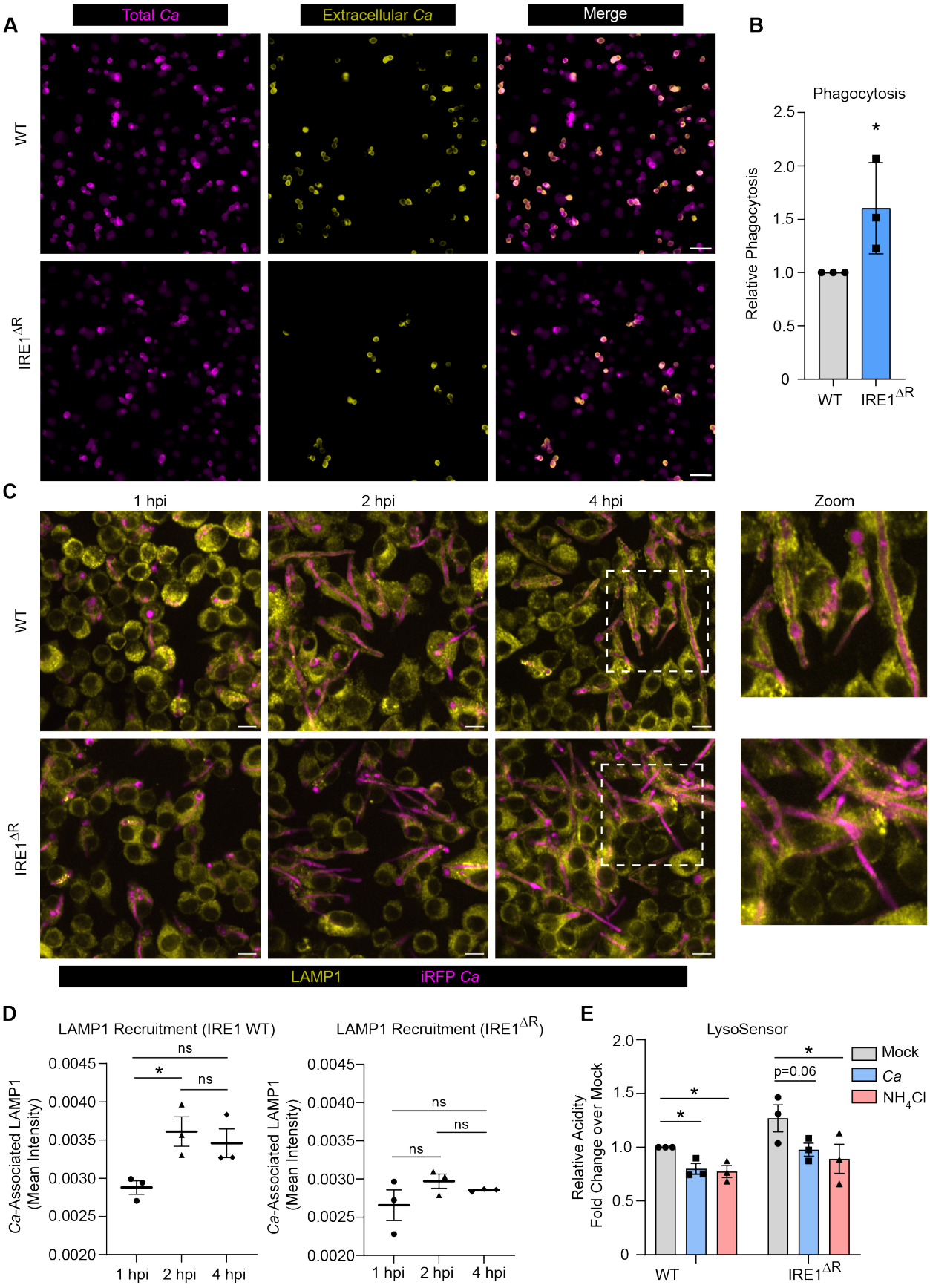
A
Total Ca
Extracellular Ca
Merge
WT
IRE1ΔR
B
Phagocytosis
Relative Phagocytosis
2.5
2.0
1.5
1.0
0.5
0
*
WT
IRE1ΔR
C
1 hpi
2 hpi
4 hpi
Zoom
WT
IRE1ΔR
LAMP1
iRFP Ca
D
LAMP1 Recruitment (IRE1 WT)
LAMP1 Recruitment (IRE1ΔR)
Ca-Associated LAMP1 (Mean Intensity)
0.0045
0.0040
0.0035
0.0030
0.0025
0.0020
ns
*
1 hpi
2 hpi
4 hpi
E
LysoSensor
Relative Acidity Fold Change over Mock
2.0
1.5
1.0
0.5
0
*
p=0.06
Mock
Ca
NH4Cl
WT
IRE1ΔR

324

325 **Figure 6: IRE1α contributes to fungal containment in the macrophage phagosome. (A)**
326 Representative phagocytosis assay micrographs show total *C. albicans* (intracellular and
327 extracellular; magenta) and extracellular *C. albicans* (yellow) following 30 minutes of phagocytosis
328 by iBMDM (IRE1 WT or IRE1$^{\Delta R}$). Scale bar 10 μm. **(B)** Quantification of 3 independent
329 phagocytosis experiments. Relative phagocytosis was calculated as fold change over IRE1 WT.
330 **(C)** Representative images showing LAMP1 (yellow) recruitment to phagosomes containing iRFP-
331 expressing *C. albicans* (magenta) in IRE1 WT or IRE1$^{\Delta R}$ iBMDM at indicated times post-infection.
332 **(D)** Quantification of LAMP1 recruitment to phagosomes containing *C. albicans* in IRE1 WT or
333 IRE1$^{\Delta R}$ iBMDM, as measured by LAMP1 mean fluorescence intensity associated with *C. albicans*-
334 expressed iRFP. **(E)** The relative acidity of IRE1 WT or IRE1$^{\Delta R}$ iBMDM following infection with *C.*
335 *albicans* or treatment with NH_4Cl as a control, shown as the relative ratio of LysoSensor intensity
336 at acidic (Excitation 384 nm, Emission 540 nm) and basic (Excitation 329 nm, Emission 440 nm)
337 conditions. Values are the mean ± SEM from 3 biological replicates. *$p < 0.05$, **$p < 0.01$, *** $p <$
338 0.001, by unpaired Student's t-test (B) or one-way ANOVA with Tukey's multiple comparisons test
339 (D, E).
340
341 **IRE1α promotes phagolysosomal fusion to constrain *C. albicans* hyphal growth and**
342 **increase fungicidal activity.**
343 As lysosome recruitment maintains the integrity of the expanding phagosome during *C.*
344 *albicans* infection[39], we reasoned that *C. albicans* may escape the phagosome more readily in
345 IRE1$^{\Delta R}$ macrophages. To test this, we used a previously-established pulse-chase assay to
346 measure phagosome leakage in which endosomes are pre-labeled with sulforhodamine B (SRB),
347 allowing fusion with *C. albicans* containing phagosomes and monitoring of phagosome rupture[39,65]
348 (Fig. 7A). Measuring SRB association with the *C. albicans*-containing phagosome over time
349 revealed that SRB was lost from the phagosome more rapidly in IRE1$^{\Delta R}$ macrophages, supporting
350 the hypothesis that IRE1α activity contributes to maintenance of the *C. albicans*-containing
351 phagosome by promoting phagolysosomal fusion (Fig. 7B). As the phagolysosomal environment
352 restricts *C. albicans* hyphal growth[66], we also measured hyphal growth over time in WT and
353 IRE1$^{\Delta R}$ macrophages and found that *C. albicans* hyphal growth is increased at 4 hpi in IRE1$^{\Delta R}$
354 macrophages (Fig. 7C).
355 Escape from the phagosome likely allows *C. albicans* to evade fungicidal effectors in
356 addition to allowing for more rapid growth. To determine whether IRE1α contributes to
357 macrophage fungicidal activity, we measured the ability of IRE1α WT and IRE1$^{\Delta R}$ macrophages
358 to kill phagocytosed *C. albicans*, using a dual fluorescence assay in which iRFP-expressing *C.*

359 *albicans* is pre-labeled with calcofluor white (CFW) prior to macrophage infection (Fig. 7D). Live
360 *C. albicans* express iRFP and are CFW labeled ($iRFP^+$ CFW^+), while killed *C. albicans* lose iRFP
361 fluorescence but can be identified by CFW labeling ($iRFP^-$ CFW^+). Using this assay, we found that
362 $IRE1^{\Delta R}$ macrophages were defective at killing phagocytosed *C. albicans*, demonstrating that
363 IRE1α activity contributes to the fungicidal activity of macrophages (Fig. 7E).
364 To determine whether failure to recruit lysosomes to the phagosome is responsible for the
365 fungicidal defect observed in $IRE1^{\Delta R}$ macrophages, we tested the effect of Bafilomycin A (BafA),
366 which inhibits vacuolar ATPase activity and thus phagosome-lysosome fusion, on the ability of
367 IRE1 WT and $IRE1^{\Delta R}$ macrophages to kill *C. albicans* (Fig. 7F). BafA treatment suppressed the
368 fungicidal activity of both IRE1 WT and $IRE1^{\Delta R}$ macrophages, reinforcing the importance of
369 phagolysosomal fusion for killing of *C. albicans*. Additionally, BafA treatment ablated the
370 difference between IRE1 WT and $IRE1^{\Delta R}$ macrophages in fungicidal capacity, demonstrating that
371 defective phagolysosomal fusion in $IRE1^{\Delta R}$ macrophages is responsible for their compromised
372 fungicidal activity (Fig. 7F). Together, these data support a model in which IRE1α activity supports
373 phagolysosomal fusion during *C. albicans* infection of macrophages to maintain phagosome
374 integrity and allow killing of ingested *C. albicans*.
375

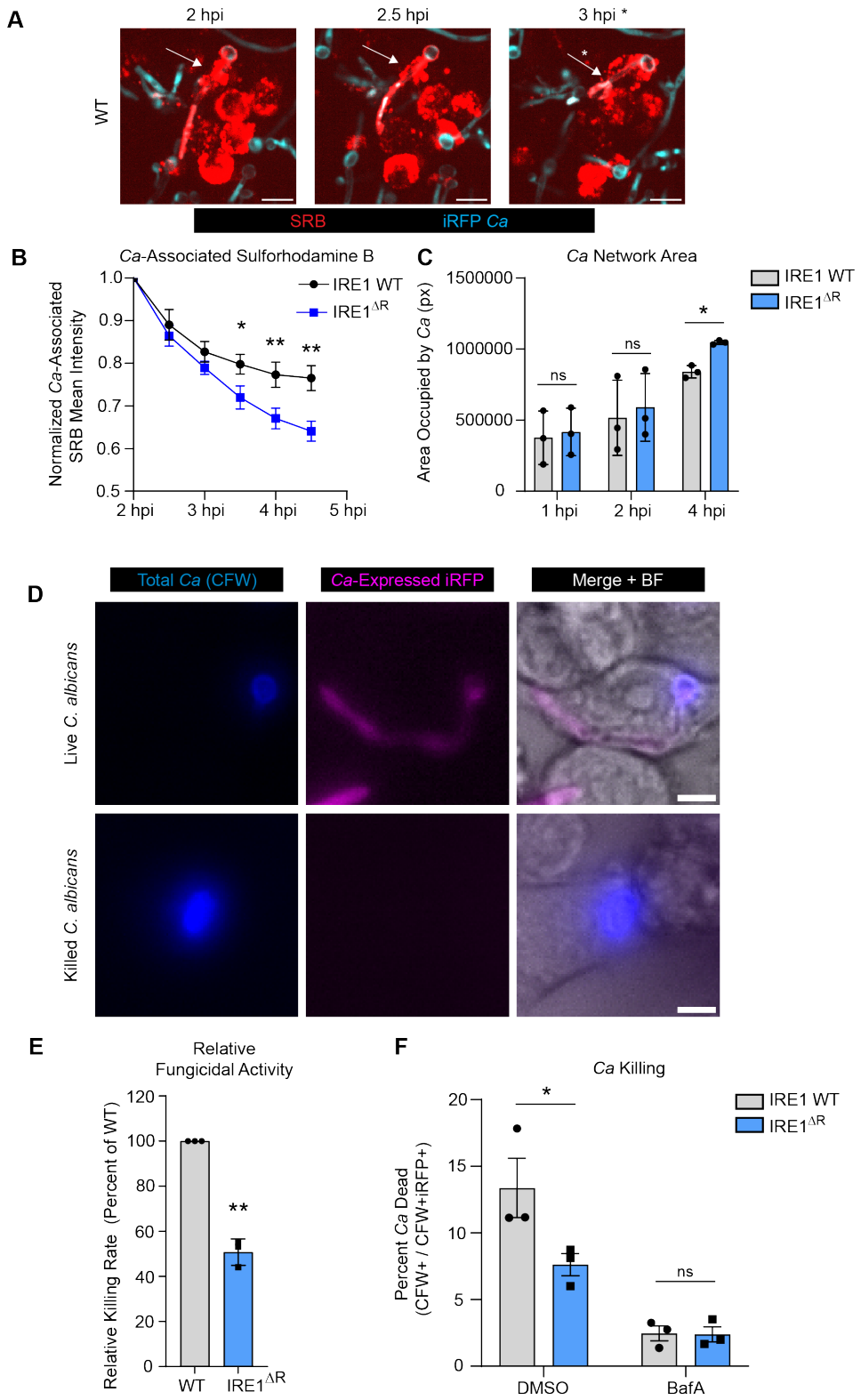

Figure 7: IRE1α promotes phagolysosomal fusion to constrain *C. albicans* hyphal growth. **(A)** Representative images of SRB recruitment to the phagosome containing *C. albicans*, indicated by white arrows, and loss of SRB association following phagosomal rupture at 3 hpi,

380 indicated by white asterisk. **(B)** Quantification of 3 independent experiments measuring the loss
381 of SRB from *C. albicans* over time in IRE1 WT or IRE1$^{\Delta R}$ iBMDM. **(C)** Quantification of the area
382 occupied (pixels) by *C. albicans* hyphae at 1, 2, and 4 hpi in IRE1 WT or IRE1$^{\Delta R}$ iBMDM. **(D)**
383 Representative micrographs of live intracellular *C. albicans* and killed intracellular *C. albicans*
384 within IRE1 WT iBMDM at 7 hpi. Endogenous expression of iRFP by *C. albicans* indicates viability
385 (CFW+ iRFP+); loss of iRFP expression indicates killed *C. albicans* (CFW+ iRFP-). Scale bar 5
386 µm. **(E)** Quantification of 3 independent *C. albicans* killing experiments (CFW+ iRFP- / CFW+
387 iRFP+), relative to WT. **(F)** Graphs show the mean ± SEM of 3 biological replicates. *$p < 0.05$, **p
388 < 0.01, by unpaired Student's t test (B, E), one-way ANOVA with Tukey's multiple comparisons
389 test (C), or two-way ANOVA with Tukey's multiple comparisons test (F).
390
391
392 **Discussion**
393 Cell and organelle stress responses are crucial regulators of innate immunity and infection
394 outcomes during bacterial and viral infection[1,2], however, the role of these stress responses in
395 antifungal innate immunity have not been explored in depth. Here, we show that *C. albicans*
396 infection of macrophages results in activation of the IRE1α branch of the mammalian ER stress
397 response. This activation is not dependent on misfolded protein stress, but instead requires
398 signaling through the CLR pathway. Interestingly, macrophages lacking IRE1α activity have
399 impaired fungicidal activity due to inefficient lysosome recruitment to the phagosome containing
400 *C. albicans*, allowing phagosomal escape by *C. albicans* and likely evasion of fungicidal effectors.
401 Together, these results demonstrate roles for IRE1α in the antifungal responses of macrophages.
402 IRE1α is activated by bacterial and viral infections, but the mechanisms driving its
403 activation are incompletely understood. While it has been suggested that innate immune signaling
404 may trigger IRE1α activation independently of misfolded protein stress, this hypothesis has not
405 been thoroughly tested. Here, we determined that CLR signaling through CARD9 triggers IRE1α
406 activation during *C. albicans* infection. Notably, measurable protein misfolding did not precede
407 IRE1α activation in response to *C. albicans* infection or LPS treatment, suggesting a potential
408 protein misfolding-independent shared mechanism of IRE1α activation downstream of innate
409 immune signaling. However, neither TLR signaling nor TRAF6 activity were required for IRE1α
410 activation during *C. albicans* infection, demonstrating that TLR and CLR signaling activate IRE1α
411 through distinct mechanisms and that *C. albicans* triggers non-canonical activation of IRE1α.
412 A potential route of IRE1α activation in the absence of misfolded protein accumulation is
413 post-translational modification, such as ubiquitination or phosphorylation [20,67]. Ubiquitination of

414 IRE1α by E3 ubiquitin ligases such as TRAF6 and CHIP contribute to IRE1α activation in
415 response to LPS treatment or geldanamycin-induced ER stress, respectively[20,68]. Additionally, the
416 endonuclease activity of IRE1α depends on its phosphorylation status, which is governed by its
417 own kinase activity, or in certain contexts may be triggered by other kinases[67]. While CLR-
418 mediated IRE1α activation occurred independently of TRAF6 activity, the CARD9-BCL10-MALT1
419 complex forms a filamentous scaffold for the assembly and activation of additional post-
420 translational modifiers, such as the kinase TAK1 and the E3 ubiquitin ligase TRAF2, which
421 interacts with IRE1α but is thought to act downstream of IRE1α[69]. Therefore, CARD9 activation
422 could facilitate interaction of IRE1α with a post-translational modifier to enable its activation.
423 Alternatively, the filamentous nature of the CARD9-BCL10-MALT1 complex could provide a
424 structural scaffold for the formation of IRE1α oligomers, which are required for its activation[15].
425 Indeed, deletion of BCL10 has previously been shown to dampen IRE1α activation in response
426 to thapsigargin-induced ER stress[70] and to be required for the pyroptotic response to *C. albicans*
427 [65]. As CARD family proteins and IRE1α have broad and overlapping functions in innate immune
428 activation and immune cell function[71,72], future work interrogating the molecular mechanisms by
429 which CARD9 triggers IRE1α activation will be of interest.

430 The convergence of TLR and CLR signaling on IRE1α activation in macrophages,
431 seemingly prior to accumulation of misfolded proteins, suggests that innate immune signaling can
432 induce anticipatory activation of IRE1α. This may serve to increase the secretory activity of
433 macrophages prior to protein misfolding for efficient innate immune responses. IRE1α activity is
434 crucial for the maturation and function of highly secretory cell types, such as plasma cells[73,74],
435 pancreatic beta cells[75], macrophages[6,76], and T cells[77]. Additionally, considering the broad roles
436 of IRE1α and XBP1S in innate immunity, including cytokine induction[6,9], metabolic plasticity[22],
437 ROS production, and microbicidal activity[11,12], proactive strategies for IRE1α activation prior to
438 protein misfolding may be important for innate immune regulation. Further elucidation of the
439 mechanisms driving protein misfolding-independent IRE1α activation will identify targets for
440 tuning of IRE1α activity, and exploration of other pathways that may trigger non-canonical
441 activation of IRE1α will help shape our understanding of IRE1α regulation.

442 Our findings also reveal a role for IRE1α in phagosome maturation during *C. albicans*
443 infection. Previous work has shown that IRE1α can be recruited to pathogen-containing
444 autophagosomes[78], and ER-phagosome contact sites can regulate phagolysosomal fusion
445 through calcium signaling[79]. Interestingly, IRE1α can function as a scaffold at ER-mitochondria
446 contact sites, allowing mitochondrial calcium uptake and regulation of cellular metabolism[24]. We
447 also observed that transcripts encoding genes involved in endocytosis and calcium signaling were

448 enriched among downregulated genes in IRE1$^{\Delta R}$ macrophages (Table S1.3), highlighting the
449 possibility that gene expression regulation by IRE1α may influence phagolysosome fusion.
450 Whether IRE1α has broad roles in phagosome-lysosome fusion, ER-phagosome contact sites, or
451 the degradative capacity of macrophages and other cell types will be an important future direction.
452 In summary, our work suggests that innate immune signaling can trigger non-canonical
453 activation of IRE1α and highlights new roles for IRE1α in the fungicidal capacity of macrophages.
454 These findings will help shape our understanding of the activation and function of IRE1α in
455 infection and other settings. Protein misfolding-independent activation of IRE1α suggests new
456 paradigms to explore in other contexts, such as sterile inflammation and obesity[80], and a critical
457 role for IRE1α as a sensor of other agents that may perturb cellular homeostasis. Dissection of
458 the molecular mechanisms regulating early IRE1α activation may identify new therapeutic targets
459 for regulation of IRE1α activity. Further, a better understanding of the role of IRE1α in the
460 endocytic pathway will provide fundamental understanding of communication between the ER
461 and endocytic compartments. Overall, these findings reveal exciting roles for a critical component
462 of the UPR during fungal infection with broad potential impacts for our understanding of cell
463 biology.
464
465
466 **Supplemental tables**
467 **Table S1: RNA-seq data from IRE1 WT and IRE1$^{\Delta R}$ macrophages infected with *C. albicans*.**
468 - **Table S1.1:** Differential gene expression in *C. albicans* infected IRE1$^{\Delta R}$ macrophages
469 compared to IRE1 WT
470 - **Table S1.2:** Gene ontology analysis of pathways enriched among genes upregulated in
471 *C. albicans* infected IRE1$^{\Delta R}$ macrophages compared to IRE1 WT
472 - **Table S1.3:** Gene ontology analysis of pathways enriched among genes downregulated
473 in *C. albicans* infected IRE1$^{\Delta R}$ macrophages compared to IRE1 WT
474 **Table S2: RNA-seq data from IRE1 WT and IRE1$^{\Delta R}$ macrophages after mock treatment.**
475 - **Table S2.1:** Differential gene expression in mock-treated IRE1$^{\Delta R}$ macrophages compared
476 to IRE1 WT
477 - **Table S2.2:** Gene ontology analysis of pathways enriched among genes upregulated in
478 mock-treated IRE1$^{\Delta R}$ macrophages compared to IRE1 WT
479 - **Table S2.3:** Gene ontology analysis of pathways enriched among genes downregulated
480 in mock-treated IRE1$^{\Delta R}$ macrophages compared to IRE1 WT
481

482
483
484 **Acknowledgements**
485 We thank the following colleagues who provided cell lines and reagents: Dr. Stacy Horner, Dr.
486 Ling Qi, Dr. Stu Levitz, Dr. Tod Merkel, and Dr. Scott Soleimanpour, as well as Dr. Jonathan
487 Sexton for microscopy equipment and advice, and Dr. Basel Abuaita for immortalization of IRE1$^{fl/fl}$
488 $^{exon20-21}$ and TLR2/4/9 knockout macrophages and matched controls. We thank members of the
489 O'Meara and O'Riordan labs for discussion. This work was supported by National Institute of
490 Health grants K22 AI137299 (T.R.O.), R01 AI157384 (M.X.D.O.), T32AR007197 (M.J.M.), and
491 T32AI007528 (M.J.M.). Other funding sources include the University of Michigan Pioneer Fellows
492 Program (M.J.M.).
493
494 **Author contributions**
495 Conceptualization: M.J.M., T.R.O., M.X.D.O., and T.R.O. Investigation: M.J.M., M.B.R.,
496 B.C.M., F.M.A. Formal analysis: M.J.M., T.R.O., M.X.D.O. Software: M.J.M., M.B.R.,
497 B.C.M, T.R.O. Writing – original draft: M.J.M., T.R.O., and M.X.D.O. Writing – review and editing:
498 M.J.M., M.B.R., B.C.M. F.M.A., M.X.D.O., and T.R.O. Funding acquisition: M.J.M., M.X.D.O., and
499 T.R.O.
500
501 **Competing interests**
502 The authors declare no competing interests.
503
504
505 **Methods**
506
507 **Plasmids.** pLEX-FLAG-Cre-GFP was generated by cloning PCR-amplified N-terminal FLAG
508 tagged Cre-GFP (from pCAG-Cre-GFP; Addgene #13776) (Forward primer:
509 TAAAGCGGCCGCTATGGCCAATTTACTGACCG; Reverse primer:
510 CTCTAGACTCGAGTTAACTTACTTGTACAGCTCGTCCA) coding sequence into the pLEX
511 expression vector using NotI and XhoI restriction sites. pLEX-FLAG-GFP vector was a gift from
512 Dr. Stacy Horner. All plasmids were verified by whole plasmid sequencing (Plasmidsaurus).
513
514 **Cell lines.** All cell lines were incubated at 37ºC with 5% CO_2. Bone marrow-derived macrophages
515 (BMDM) were grown in bone marrow media (BMM), containing modification of Eagle's medium

516 (DMEM; Thermo Fisher Scientific) supplemented with 20% fetal bovine serum (Thermo Fisher
517 Scientific), 30% L929 conditioned media, and 1 mM sodium pyruvate (Thermo Fisher Scientific).
518 BMDM were immortalized (iBMDM) using J2 retrovirus[82]. L-929 cells were cultured in minimum
519 essential Eagle's medium supplemented with 2 mM l-glutamine, 1 mM sodium pyruvate, 1 mM
520 nonessential amino acid, 10 mM HEPES, and 10% FBS. All experiments were performed in
521 experimental media (RPMI supplemented with 3% FBS) unless otherwise indicated. All cell lines
522 were verified as mycoplasma free using the Lookout Mycoplasma PCR Detection Kit (Sigma-
523 Aldrich) and genetic identities were validated by PCR, western blotting, or functional assays.
524 $IRE1^{fl/fl\ exon20\text{-}21}$ (-/+ Cre) mice were a gift from Dr. Ling Qi, CARD9 knockout macrophages and
525 littermate WT mice were a gift from Dr. Stu Levitz, TLR2/4/9 knockout mice and littermate WT
526 mice were a gift from Dr. Tod Merkel, and $TRAF6^{fl/fl}$ mice were a gift from Dr. Scott Soleimanpour.
527 To generate $IRE1^{\Delta R}$ and control IRE1 WT macrophages, iBMDM from $IRE1^{fl/fl\ exon20\text{-}21}$ mice with
528 and without inducible Cre expression were treated with 4-hydroxy tamoxifen for 24 hours, followed
529 by clonal expansion of cell lines. $IRE1^{\Delta R}$ macrophages were confirmed by macrophages and *Xbp1*
530 splicing assays. To generate TRAF6 KO cell lines, first lentiviral particles encoding GFP or CRE-
531 GFP were generated by harvesting supernatant 72 h post-transfection of 293T cells with pLEX-
532 FLAG-GFP, or pLEX-FLAG-Cre-GFP, and the packaging plasmids psPAX2 and pMD2.G
533 (provided by Dr. Stacy Horner). These supernatants were then used to transduce $TRAF6^{fl/fl}$
534 iBMDM for 24 hours. Following transduction, cells were selected in 3 µg/mL puromycin (Sigma)
535 for 48 hours and then single cell colonies were isolated. Overexpression of FLAG-tagged proteins
536 in selected colonies was verified by immunoblotting, and TRAF6 deletion in CRE-GFP cell lines
537 was verified by immunoblotting. This yielded generation of GFP-expressing $TRAF6^{fl/fl}$ iBMDM
538 clonal cell lines as a control (WT-1 and WT-2) or CRE-GFP expressing $TRAF6^{fl/fl}$ iBMDM clonal
539 cell lines (KO-1 and KO-2).
540
541 ***Candida albicans* infection and LPS treatment.** *C. albicans* cells were cultured at 30 °C in YPD
542 liquid media (1% yeast extract, 2% peptone, 2% dextrose) with constant agitation. All strains were
543 maintained as frozen stocks of 25% glycerol at -80 °C. For infection of iBMDM, macrophages
544 were seeded in experimental plates overnight at approximately 80% confluence. Experimental
545 media (RPMI (Gibco), supplemented with 3% FBS) was inoculated with log-phase *C. albicans*
546 cells counted for a calculated MOI of 1. LPS from *E. coli* O111:B4 (Sigma-Aldrich L2630) was
547 diluted to 100 ng/mL in experimental media for all experiments.
548

549 **RT-qPCR.** Total cellular RNA was extracted from all samples using TRIzol (Thermo Fisher
550 Scientific), according to manufacturer protocol. RNA was then reverse transcribed using the
551 iScript cDNA synthesis kit (Bio-Rad) as per the manufacturer's instructions. The resulting cDNA
552 was diluted 1:5 in nuclease-free H2O. RT-qPCR was performed in triplicate using the PowerUP
553 SYBR Green PCR master mix (Thermo Fisher Scientific) and the Bio-Rad CFX Opus 384 Real-
554 Time RT-PCR systems. *Xbp1-S* transcript was amplified using primers Forward:
555 GCTGAGTCCGCAGCAGGT and Reverse: CAGGGTCCAACTTGTCCAGAAT. *Gapdh* transcript
556 was amplified using primers Forward: CATCACTGCCACCCAGAAGACTG and Reverse:
557 ATGCCAGTGAGCTTCCCGTTCAG.
558
559 **Semi-quantitative *Xbp1* Splicing Gel Analysis.** Total cellular RNA was extracted using TRIzol
560 (Thermo Fisher Scientific), according to manufacturer protocol. RNA was then reverse transcribed
561 using the iScript cDNA synthesis kit (Bio-Rad) as per the manufacturer's instructions. The
562 resulting cDNA was diluted 1:5 in nuclease-free H2O. *Xbp1* transcript was amplified by PCR using
563 primers XF and XR, followed by PCR cleanup using the Qiagen PCR Cleanup Kit. The amplified
564 *Xbp1* product was then digested using PstI, which recognizes a cleavage site within the 26 base
565 pair intron that is removed by IRE1α activity[82]. Following digestion, *Xbp1* bands were resolved on
566 a 2% agarose gel and visualized by ethidium bromide staining and imaging on a BioRad gel dock.
567
568 **Immunoblotting.** Cells were lysed in a modified radioimmunoprecipitation assay (RIPA) buffer
569 (10 mM Tris [pH 7.5], 150 mM NaCl, 0.5% sodium deoxycholate, and 1% Triton X-100)
570 supplemented with protease and phosphatase inhibitor cocktail (Millipore-Sigma) and post-
571 nuclear lysates were harvested by centrifugation. Quantified protein (between 5 and 15 mg) was
572 added to a 4X SDS protein sample buffer (40% glycerol, 240 mM Tris-HCl [pH 6.8], 8% SDS,
573 0.04% bromophenol blue, 5% beta-mercaptoethanol), resolved by SDS/PAGE, and transferred
574 to nitrocellulose membranes in a 25 mM Tris-192 mM glycine-0.01% SDS buffer. Membranes
575 were stained with Revert 700 total protein stain (LI-COR Biosciences), then blocked in 3% bovine
576 serum albumin. Membranes were incubated with primary antibodies for 2 hours at room
577 temperature or overnight at 4C. After washing with PBS-T buffer (1 3 PBS, 0.05% Tween 20),
578 membranes were incubated with species-specific IRDye-conjugated antibodies (Licor, 1:5000) for
579 1 hour at room temperature, followed by imaging on an Odyssey imaging system (LI-COR
580 Biosciences). The following antibodies were used for immunoblotting: rabbit anti-IRE1α
581 (CellSignaling 3924, 1:1000); rabbit anti-XBP1 (Abcam AB-37152, 1:1000); mouse anti-ACTIN

582 (ThermoFisher ACTN05 (C4), 1:5000); rabbit anti-TRAF6 (Abcam ab40675, 1:1000); rabbit anti-
583 CARD9 (CellSignaling 12283, 1:1000).
584
585 **Quantification of Immunoblots.** Following imaging using the LI-COR Odyssey imager,
586 immunoblots were quantified using ImageStudio Lite software, and raw values were normalized
587 to total protein (Revert 700 total protein stain) or ACTIN for each condition.
588
589 **Thioflavin T Assay.** iBMDM ($2*10^5$ cells/well) were seeded in a 24-well plate overnight and then
590 infected with *C. albicans*, or treated with LPS or thapsigargin for indicated timepoints. Thioflavin
591 T (Cayman Chemical, 5 μM) was added 2 hours prior to endpoint. Cells were scraped into ice
592 cold PBS and thioflavin T intensity was measured on a BD LSRFortessa X-20 flow cytometer.

593 **RNA-sequencing.** iBMDM were seeded in 6-well plates overnight (10^6 cells/well) then infected
594 with *C. albicans* (MOI 1) or mock treated (4 h), then harvested in TRIzol reagent (Thermo Fisher)
595 and RNA extraction was performed according to manufacturer protocol. Samples were then
596 treated with Turbo DNase I (Thermo Fisher) according to manufacturer protocol and incubated at
597 37 ˚C for 30 min, followed by phenol/chloroform extraction and ethanol precipitation overnight.
598 RNA concentrations were then normalized. PolyA enrichment was performed and sequencing
599 libraries were prepared and sequenced on an Illumina NovaSeq 6000 with 150 bp paired-end
600 reads by Novogene.

601 **RNA-seq analysis.** RNA-seq analysis was performed in Galaxy (usegalaxy.org). Reads were
602 evaluated using FastQC and trimmed using cutadapt[83], followed by quantification of transcripts
603 from the GRCm38 mouse genome using Kallisto[84]. Differential gene expression between $IRE1^{\Delta R}$
604 and IRE1 WT macrophages following *C. albicans* infection (Table S1.1) or mock treatment (Table
605 S2.1) were compared using DESeq2[85]. Gene ontology analysis was performed on significantly
606 upregulated or downregulated genes in each data set using GProfiler.

607
608 **ELISA.** iBMDM ($3*10^4$ cells/well) were seeded in 96-well plates overnight, then primed with LPS
609 (100 ng/mL) for 3 hours prior to *C. albicans* infection (MOI 1). Supernatants were collected at 5
610 hpi and submitted to the University of Michigan Cancer Center Immunology Core for quantification
611 of secreted IL-1β, TNF, and IL-6.
612

613 **Quantification of Phagocytosis of *C. albicans*.** iBMDM ($3*10^4$ cells/well) were seeded in a 96-
614 well plastic-bottom imaging plate (PerkinElmer) overnight and then infected with *C. albicans* (MOI
615 1) for 30 minutes. Wells were then fixed in 4% parafolmaldehyde (Electron Microscopy Sciences)
616 for 15 minutes, washed with PBS (ThermoFisher), and blocked with PBS containing 3% bovine
617 serum albumin (ThermoFisher) and 5% normal goat serum (Invitrogen) for 30 minutes. FITC-
618 conjugated anti-*Candida* antibody (LSBio LS-C103355, 1:2000) was diluted in blocking buffer and
619 added for 1 hour with agitation to label extracellular *C. albicans*, followed by 3 5 minute washes
620 with PBS. Wells were then permeabilized in 0.1% Triton-X 100 (Sigma-Aldrich) for 15 minutes,
621 followed by 3 washes in PBS. Calcofluor white (Sigma-Aldrich, 1:100) was diluted in blocking
622 buffer and added to wells for 30 minutes with agitation, followed by 3 5 minute PBS washes, and
623 images were captured on a BioTek Lionheart FX automated microscope. A CellProfiler pipeline
624 was developed to segment extracellular (FITC+) and total (FITC+ CFW+) *C. albicans*, and the
625 percent phagocytosed by macrophages was calculated as 100 * (1 – (FITC+ / FITC+ CFW+)).
626
627 **Quantification of phagolysosomal fusion.** iBMDM ($3*10^4$ cells/well) were seeded in a 96-well
628 plastic-bottom imaging plate (PerkinElmer) overnight and then infected with *C. albicans* SC5314
629 cells expressing near-infrared fluorescent protein (iRFP) driven by the ENO1 promoter[86] (MOI 1)
630 at indicated timepoints. Wells were then fixed in 4% parafolmaldehyde (Electron Microscopy
631 Sciences) for 15 minutes, washed with PBS (ThermoFisher), and permeabilized in 0.1% Triton-X
632 100 (Sigma-Aldrich) for 15 minutes, followed by 3 washes in PBS. Wells were blocked with PBS
633 containing 0.01% Triton-X 100, 3% bovine serum albumin (ThermoFisher) and 5% normal goat
634 serum (Invitrogen) for 30 minutes. Primary antibodies rat anti-LAMP1 (DSHB 1D4B, 1:50) and
635 rabbit anti-LC3 (MBL pM036, 1:400) were diluted in block buffer and added to wells for 1 hour,
636 followed by 3 5 minute washes with PBS. Alexafluor-conjugated secondary antibodies goat anti-
637 rat 594 and goat anti-rabbit 488 were diluted 1:500 in blocking buffer with DAPI (1:1000) and
638 added to wells for 1 hour, followed by 3 5 minute PBS washes, and images were captured on a
639 Yokogawa CellVoyager CQ1 automated confocal microscope. A CellProfiler pipeline was
640 developed to segment *C. albicans* and measure the mean intensity of LAMP1 enriched at the *C.*
641 *albicans* network.
642
643 **Macrophage Fungicidal Activity Assay.** iBMDM ($3*10^4$ cells/well) were seeded in a 96-well
644 plastic-bottom imaging plate (PerkinElmer) overnight. Approximately 10^7 *C. albicans* SC5314
645 cells expressing iRFP from an overnight culture were stained with calcofluor white (CFW; 100
646 µg/mL) for 10 minutes in the dark. Cells were then washed twice with PBS prior to macrophage

647 infection at MOI = 1. Images of infected cultures were captured every 20 minutes on a BioTek
648 Lionheart FX automated microscope with incubation at 37C and 5% CO2. Fungal killing was
649 quantified at 7 hours post-infection by calculating killed *C. albicans* (iRFP^{-} CFW^{+}) over total *C.*
650 *albicans* (iRFP$^{-/+}$ CFW^{+}), with at least 200 *C. albicans* cells counted per condition.
651
652 **LysoSensor.** iBMDM (2*10^{5} cells/well) were seeded in a 24-well plate overnight and then infected
653 with *C. albicans* for 2 hours prior to addition of LysoSensor Yellow/Blue DND-160 (Thermo Fisher,
654 500 nM) for 2 minutes in experimental media. Wells were then washed 3 times in ice-cold PBS
655 and scraped for plate reader analysis. Suspended cells were added to a black-bottom 96-well
656 plate and absorbance and emission were measured at 329nm Abs, 440nm Em and 384nm Abs,
657 540nm Em to measure fluorescence intensity in high and low pH environments, respectively. The
658 intensity of the low pH measurement was divided by the intensity of the high pH measurement,
659 and these results were normalized to IRE1 WT Mock to determine the relative acidity of each
660 condition.
661
662 **Sulforhodamine B Assay and *C. albicans* hyphal length measurement.** iBMDM (3*10^{4}
663 cells/well) were seeded in a 96-well plastic-bottom imaging plate (PerkinElmer) overnight, then
664 sulforhodamine B (SRB) (Sigma-Aldrich, 150 ug/mL) was added to wells for 1 hour. SRB was
665 then washed out and wells were with *C. albicans* expressing iRFP (MOI 1) and live imaging was
666 performed on a Yokogawa CellVoyager CQ1 automated confocal microscope every 30 minutes
667 for 5 hours. A CellProfiler pipeline was developed to segment *C. albicans* and measure the total
668 area covered by hyphae, and the mean intensity of SRB enriched at the *C. albicans* network was
669 measured at each timepoint.
670
671
672 **Lead Contact and Materials Availability**. Further information and requests for resources and
673 reagents should be directed to and will be fulfilled by the Lead Contacts, Teresa O'Meara
674 (tromeara@umich.edu) and/or Mary O'Riordan (oriordan@umich.edu)
675
676 **Data Availability.** All raw data related to RNA-seq are available through GEO (accession number:
677 GSE244303). All raw data related to microscopy are available upon request.
678
679 **Code Availability.** CellProfiler pipelines for image quantification are available as Supplementary
680 Materials (files S3-S5).

683 **References**

684

685 1. Muralidharan, S., and Mandrekar, P. (2013). Cellular stress response and innate immune
686 signaling: integrating pathways in host defense and inflammation. J. Leukoc. Biol. *94*, 1167–
687 1184.
688 2. Chovatiya, R., and Medzhitov, R. (2014). Stress, inflammation, and defense of homeostasis.
689 Mol. Cell *54*, 281–288.
690 3. Grootjans, J., Kaser, A., Kaufman, R.J., and Blumberg, R.S. (2016). The unfolded protein
691 response in immunity and inflammation. Nat. Rev. Immunol. *16*, 469–484.
692 4. Choi, J.-A., and Song, C.-H. (2019). Insights Into the Role of Endoplasmic Reticulum Stress
693 in Infectious Diseases. Front. Immunol. *10*, 3147.
694 5. Read, A., and Schröder, M. (2021). The Unfolded Protein Response: An Overview. Biology
695 *10*. 10.3390/biology10050384.
696 6. Martinon, F., Chen, X., Lee, A.-H., and Glimcher, L.H. (2010). TLR activation of the
697 transcription factor XBP1 regulates innate immune responses in macrophages. Nat.
698 Immunol. *11*, 411–418.
699 7. Watowich, S.S., Morimoto, R.I., and Lamb, R.A. (1991). Flux of the paramyxovirus
700 hemagglutinin-neuraminidase glycoprotein through the endoplasmic reticulum activates
701 transcription of the GRP78-BiP gene. J. Virol. *65*, 3590–3597.
702 8. Tardif, K.D., Mori, K., Kaufman, R.J., and Siddiqui, A. (2004). Hepatitis C virus suppresses
703 the IRE1-XBP1 pathway of the unfolded protein response. J. Biol. Chem. *279*, 17158–17164.
704 9. Bronner, D.N., Abuaita, B.H., Chen, X., Fitzgerald, K.A., Nuñez, G., He, Y., Yin, X.-M., and
705 O'Riordan, M.X.D. (2015). Endoplasmic Reticulum Stress Activates the Inflammasome via
706 NLRP3- and Caspase-2-Driven Mitochondrial Damage. Immunity *43*, 451–462.
707 10. Baruch, M., Hertzog, B.B., Ravins, M., Anand, A., Cheng, C.Y., Biswas, D., Tirosh, B., and
708 Hanski, E. (2014). Induction of endoplasmic reticulum stress and unfolded protein response
709 constitutes a pathogenic strategy of group A streptococcus. Front. Cell. Infect. Microbiol. *4*,
710 105.
711 11. Abuaita, B.H., Burkholder, K.M., Boles, B.R., and O'Riordan, M.X. (2015). The Endoplasmic
712 Reticulum Stress Sensor Inositol-Requiring Enzyme 1α Augments Bacterial Killing through
713 Sustained Oxidant Production. MBio *6*, e00705.
714 12. Abuaita, B.H., Schultz, T.L., and O'Riordan, M.X. (2018). Mitochondria-Derived Vesicles
715 Deliver Antimicrobial Reactive Oxygen Species to Control Phagosome-Localized
716 Staphylococcus aureus. Cell Host Microbe *24*, 625-636.e5.
717 13. Awasthi, D., Chopra, S., Cho, B.A., Emmanuelli, A., Sandoval, T.A., Hwang, S.-M., Chae,
718 C.-S., Salvagno, C., Tan, C., Vasquez-Urbina, L., et al. (2023). Inflammatory ER stress
719 responses dictate the immunopathogenic progression of systemic candidiasis. J. Clin.
720 Invest. 10.1172/JCI167359.
721 14. Celli, J., and Tsolis, R.M. (2015). Bacteria, the endoplasmic reticulum and the unfolded
722 protein response: friends or foes? Nat. Rev. Microbiol. *13*, 71–82.
723 15. Belyy, V., Zuazo-Gaztelu, I., Alamban, A., Ashkenazi, A., and Walter, P. (2022). Endoplasmic
724 reticulum stress activates human IRE1α through reversible assembly of inactive dimers into
725 small oligomers. Elife *11*. 10.7554/eLife.74342.
726 16. Yoshida, H., Matsui, T., Yamamoto, A., Okada, T., and Mori, K. (2001). XBP1 mRNA is
727 induced by ATF6 and spliced by IRE1 in response to ER stress to produce a highly active
728 transcription factor. Cell *107*, 881–891.
729 17. Cox, J.S., and Walter, P. (1996). A novel mechanism for regulating activity of a transcription
730 factor that controls the unfolded protein response. Cell *87*, 391–404.
731 18. Kaufman, R.J. (1999). Stress signaling from the lumen of the endoplasmic reticulum:
732 coordination of gene transcriptional and translational controls. Genes Dev. *13*, 1211–1233.

19. Park, S.-M., Kang, T.-I., and So, J.-S. (2021). Roles of XBP1s in Transcriptional Regulation of Target Genes. Biomedicines *9*. 10.3390/biomedicines9070791.
20. Qiu, Q., Zheng, Z., Chang, L., Zhao, Y.-S., Tan, C., Dandekar, A., Zhang, Z., Lin, Z., Gui, M., Li, X., et al. (2013). Toll-like receptor-mediated IRE1α activation as a therapeutic target for inflammatory arthritis. EMBO J. *32*, 2477–2490.
21. Nguyen, L.C., Renner, D.M., Silva, D., Yang, D., Parenti, N., Medina, K.M., Nicolaescu, V., Gula, H., Drayman, N., Valdespino, A., et al. (2022). SARS-CoV-2 diverges from other betacoronaviruses in only partially activating the IRE1α/XBP1 ER stress pathway in human lung-derived cells. bioRxiv. 10.1101/2021.12.30.474519.
22. English, B.C., Savage, H.P., Mahan, S.P., Diaz-Ochoa, V.E., Young, B.M., Abuaita, B.H., Sule, G., Knight, J.S., O'Riordan, M.X., Bäumler, A.J., et al. (2023). The IRE1α-XBP1 Signaling Axis Promotes Glycolytic Reprogramming in Response to Inflammatory Stimuli. MBio *14*, e0306822.
23. Yu, C.-Y., Hsu, Y.-W., Liao, C.-L., and Lin, Y.-L. (2006). Flavivirus infection activates the XBP1 pathway of the unfolded protein response to cope with endoplasmic reticulum stress. J. Virol. *80*, 11868–11880.
24. Carreras-Sureda, A., Jaña, F., Urra, H., Durand, S., Mortenson, D.E., Sagredo, A., Bustos, G., Hazari, Y., Ramos-Fernández, E., Sassano, M.L., et al. (2019). Non-canonical function of IRE1α determines mitochondria-associated endoplasmic reticulum composition to control calcium transfer and bioenergetics. Nat. Cell Biol. *21*, 755–767.
25. Anderson, F.M., Visser, N.D., Amses, K.R., Hodgins-Davis, A., Weber, A.M., Metzner, K.M., McFadden, M.J., Mills, R.E., O'Meara, M.J., James, T.Y., et al. (2023). Candida albicans selection for human commensalism results in substantial within-host diversity without decreasing fitness for invasive disease. PLoS Biol. *21*, e3001822.
26. Lionakis, M.S., Swamydas, M., Fischer, B.G., Plantinga, T.S., Johnson, M.D., Jaeger, M., Green, N.M., Masedunskas, A., Weigert, R., Mikelis, C., et al. (2013). CX3CR1-dependent renal macrophage survival promotes Candida control and host survival. J. Clin. Invest. *123*, 5035–5051.
27. Martino, P., Girmenia, C., Venditti, M., Micozzi, A., Santilli, S., Burgio, V.L., and Mandelli, F. (1989). Candida colonization and systemic infection in neutropenic patients. A retrospective study. Cancer *64*, 2030–2034.
28. Netea, M.G., Brown, G.D., Kullberg, B.J., and Gow, N.A.R. (2008). An integrated model of the recognition of Candida albicans by the innate immune system. Nat. Rev. Microbiol. *6*, 67–78.
29. McKenzie, C.G.J., Koser, U., Lewis, L.E., Bain, J.M., Mora-Montes, H.M., Barker, R.N., Gow, N.A.R., and Erwig, L.P. (2010). Contribution of Candida albicans cell wall components to recognition by and escape from murine macrophages. Infect. Immun. *78*, 1650–1658.
30. Qian, Q., Jutila, M.A., Van Rooijen, N., and Cutler, J.E. (1994). Elimination of mouse splenic macrophages correlates with increased susceptibility to experimental disseminated candidiasis. J. Immunol. *152*, 5000–5008.
31. Hise, A.G., Tomalka, J., Ganesan, S., Patel, K., Hall, B.A., Brown, G.D., and Fitzgerald, K.A. (2009). An essential role for the NLRP3 inflammasome in host defense against the human fungal pathogen Candida albicans. Cell Host Microbe *5*, 487–497.
32. Joly, S., Ma, N., Sadler, J.J., Soll, D.R., Cassel, S.L., and Sutterwala, F.S. (2009). Cutting edge: Candida albicans hyphae formation triggers activation of the Nlrp3 inflammasome. J. Immunol. *183*, 3578–3581.
33. Gross, O., Poeck, H., Bscheider, M., Dostert, C., Hannesschläger, N., Endres, S., Hartmann, G., Tardivel, A., Schweighoffer, E., Tybulewicz, V., et al. (2009). Syk kinase signalling couples to the Nlrp3 inflammasome for anti-fungal host defence. Nature *459*, 433–436.
34. Wellington, M., Koselny, K., and Krysan, D.J. (2012). Candida albicans morphogenesis is not required for macrophage interleukin 1β production. MBio *4*, e00433-12.

35. Wellington, M., Koselny, K., Sutterwala, F.S., and Krysan, D.J. (2014). Candida albicans triggers NLRP3-mediated pyroptosis in macrophages. Eukaryot. Cell *13*, 329–340.
36. O'Meara, T.R., Veri, A.O., Ketela, T., Jiang, B., Roemer, T., and Cowen, L.E. (2015). Global analysis of fungal morphology exposes mechanisms of host cell escape. Nat. Commun. *6*, 6741.
37. Diamond, R.D., Lyman, C.A., and Wysong, D.R. (1991). Disparate effects of interferon-gamma and tumor necrosis factor-alpha on early neutrophil respiratory burst and fungicidal responses to Candida albicans hyphae in vitro. J. Clin. Invest. *87*, 711–720.
38. Newman, S.L., Bhugra, B., Holly, A., and Morris, R.E. (2005). Enhanced killing of Candida albicans by human macrophages adherent to type 1 collagen matrices via induction of phagolysosomal fusion. Infect. Immun. *73*, 770–777.
39. Westman, J., Walpole, G.F.W., Kasper, L., Xue, B.Y., Elshafee, O., Hube, B., and Grinstein, S. (2020). Lysosome Fusion Maintains Phagosome Integrity during Fungal Infection. Cell Host Microbe *28*, 798-812.e6.
40. Seegren, P.V., Downs, T.K., Stremska, M.E., Harper, L.R., Cao, R., Olson, R.J., Upchurch, C.M., Doyle, C.A., Kennedy, J., Stipes, E.L., et al. (2020). Mitochondrial Ca2 Signaling Is an Electrometabolic Switch to Fuel Phagosome Killing. Cell Reports *33*, 108411. 10.1016/j.celrep.2020.108411.
41. Vesely, E.M., Williams, R.B., Konopka, J.B., and Lorenz, M.C. (2017). N-Acetylglucosamine Metabolism Promotes Survival of Candida albicans in the Phagosome. mSphere *2*. 10.1128/mSphere.00357-17.
42. Iwawaki, T., Akai, R., Yamanaka, S., and Kohno, K. (2009). Function of IRE1 alpha in the placenta is essential for placental development and embryonic viability. Proc. Natl. Acad. Sci. U. S. A. *106*, 16657–16662.
43. Glazier, V.E., Kramara, J., Ollinger, T., Solis, N.V., Zarnowski, R., Wakade, R.S., Kim, M.-J., Weigel, G.J., Liang, S.-H., Bennett, R.J., et al. (2023). The Candida albicans reference strain SC5314 contains a rare, dominant allele of the transcription factor Rob1 that modulates filamentation, biofilm formation, and oral commensalism. MBio, e0152123.
44. Hardison, S.E., and Brown, G.D. (2012). C-type lectin receptors orchestrate antifungal immunity. Nat. Immunol. *13*, 817–822.
45. Poltorak, A., Smirnova, I., He, X., Liu, M.Y., Van Huffel, C., McNally, O., Birdwell, D., Alejos, E., Silva, M., Du, X., et al. (1998). Genetic and physical mapping of the Lps locus: identification of the toll-4 receptor as a candidate gene in the critical region. Blood Cells Mol. Dis. *24*, 340–355.
46. Hsu, Y.-M.S., Zhang, Y., You, Y., Wang, D., Li, H., Duramad, O., Qin, X.-F., Dong, C., and Lin, X. (2007). The adaptor protein CARD9 is required for innate immune responses to intracellular pathogens. Nat. Immunol. *8*, 198–205.
47. Netea, M.G., Van Der Graaf, C.A.A., Vonk, A.G., Verschueren, I., Van Der Meer, J.W.M., and Kullberg, B.J. (2002). The role of toll-like receptor (TLR) 2 and TLR4 in the host defense against disseminated candidiasis. J. Infect. Dis. *185*, 1483–1489.
48. Kawai, T., and Akira, S. (2010). The role of pattern-recognition receptors in innate immunity: update on Toll-like receptors. Nat. Immunol. *11*, 373–384.
49. Gorjestani, S., Darnay, B.G., and Lin, X. (2012). Tumor necrosis factor receptor-associated factor 6 (TRAF6) and TGFβ-activated kinase 1 (TAK1) play essential roles in the C-type lectin receptor signaling in response to Candida albicans infection. J. Biol. Chem. *287*, 44143–44150.
50. Beriault, D.R., and Werstuck, G.H. (2013). Detection and quantification of endoplasmic reticulum stress in living cells using the fluorescent compound, Thioflavin T. Biochim. Biophys. Acta *1833*, 2293–2301.
51. Hollien, J., and Weissman, J.S. (2006). Decay of endoplasmic reticulum-localized mRNAs during the unfolded protein response. Science *313*, 104–107.

835 52. Hollien, J., Lin, J.H., Li, H., Stevens, N., Walter, P., and Weissman, J.S. (2009). Regulated
836 Ire1-dependent decay of messenger RNAs in mammalian cells. J. Cell Biol. *186*, 323–331.
837 53. Upton, J.-P., Wang, L., Han, D., Wang, E.S., Huskey, N.E., Lim, L., Truitt, M., McManus,
838 M.T., Ruggero, D., Goga, A., et al. (2012). IRE1α cleaves select microRNAs during ER stress
839 to derepress translation of proapoptotic Caspase-2. Science *338*, 818–822.
840 54. Acosta-Alvear, D., Karagöz, G.E., Fröhlich, F., Li, H., Walther, T.C., and Walter, P. (2018).
841 The unfolded protein response and endoplasmic reticulum protein targeting machineries
842 converge on the stress sensor IRE1. Elife *7*. 10.7554/eLife.43036.
843 55. Shaw, A.E., Hughes, J., Gu, Q., Behdenna, A., Singer, J.B., Dennis, T., Orton, R.J., Varela,
844 M., Gifford, R.J., Wilson, S.J., et al. (2017). Fundamental properties of the mammalian innate
845 immune system revealed by multispecies comparison of type I interferon responses. PLoS
846 Biol. *15*, e2004086.
847 56. Tufanli, O., Telkoparan Akillilar, P., Acosta-Alvear, D., Kocaturk, B., Onat, U.I., Hamid, S.M.,
848 Çimen, I., Walter, P., Weber, C., and Erbay, E. (2017). Targeting IRE1 with small molecules
849 counteracts progression of atherosclerosis. Proc. Natl. Acad. Sci. U. S. A. *114*, E1395–
850 E1404.
851 57. Chan, S.M.H., Lowe, M.P., Bernard, A., Miller, A.A., and Herbert, T.P. (2018). The inositol-
852 requiring enzyme 1 (IRE1α) RNAse inhibitor, 4μ8C, is also a potent cellular antioxidant.
853 Biochem. J *475*, 923–929.
854 58. Nakajima, S., and Kitamura, M. (2013). Bidirectional regulation of NF-κB by reactive oxygen
855 species: a role of unfolded protein response. Free Radic. Biol. Med. *65*, 162–174.
856 59. Yates, R.M., Hermetter, A., Taylor, G.A., and Russell, D.G. (2007). Macrophage activation
857 downregulates the degradative capacity of the phagosome. Traffic *8*, 241–250.
858 60. Trost, M., English, L., Lemieux, S., Courcelles, M., Desjardins, M., and Thibault, P. (2009).
859 The phagosomal proteome in interferon-gamma-activated macrophages. Immunity *30*, 143–
860 154.
861 61. Sakurai, C., Itakura, M., Kinoshita, D., Arai, S., Hashimoto, H., Wada, I., and Hatsuzawa, K.
862 (2018). Phosphorylation of SNAP-23 at Ser95 causes a structural alteration and negatively
863 regulates Fc receptor–mediated phagosome formation and maturation in macrophages. Mol.
864 Biol. Cell *29*, 1753–1762.
865 62. Vylkova, S., and Lorenz, M.C. (2014). Modulation of phagosomal pH by Candida albicans
866 promotes hyphal morphogenesis and requires Stp2p, a regulator of amino acid transport.
867 PLoS Pathog. *10*, e1003995.
868 63. Danhof, H.A., and Lorenz, M.C. (2015). The Candida albicans ATO Gene Family Promotes
869 Neutralization of the Macrophage Phagolysosome. Infect. Immun. *83*, 4416–4426.
870 64. Boron, W.F., and De Weer, P. (1976). Intracellular pH transients in squid giant axons caused
871 by CO2, NH3, and metabolic inhibitors. J. Gen. Physiol. *67*, 91–112.
872 65. O'Meara, T.R., Duah, K., Guo, C.X., Maxson, M.E., Gaudet, R.G., Koselny, K., Wellington,
873 M., Powers, M.E., MacAlpine, J., O'Meara, M.J., et al. (2018). High-Throughput Screening
874 Identifies Genes Required for Candida albicans Induction of Macrophage Pyroptosis. MBio
875 *9*. 10.1128/mBio.01581-18.
876 66. Yang, M., Walpole, G.F.W., and Westman, J. (2020). Maintaining phagosome integrity
877 during fungal infection: do or die? Microb. Cell Fact. *7*, 323–325.
878 67. Dufey, E., Bravo-San Pedro, J.M., Eggers, C., González-Quiroz, M., Urra, H., Sagredo, A.I.,
879 Sepulveda, D., Pihán, P., Carreras-Sureda, A., Hazari, Y., et al. (2020). Genotoxic stress
880 triggers the activation of IRE1α-dependent RNA decay to modulate the DNA damage
881 response. Nat. Commun. *11*, 2401.
882 68. Zhu, X., Zhang, J., Sun, H., Jiang, C., Dong, Y., Shan, Q., Su, S., Xie, Y., Xu, N., Lou, X., et
883 al. (2014). Ubiquitination of inositol-requiring enzyme 1 (IRE1) by the E3 ligase CHIP
884 mediates the IRE1/TRAF2/JNK pathway. J. Biol. Chem. *289*, 30567–30577.

885 69. Urano, F., Wang, X., Bertolotti, A., Zhang, Y., Chung, P., Harding, H.P., and Ron, D. (2000).
886 Coupling of stress in the ER to activation of JNK protein kinases by transmembrane protein
887 kinase IRE1. Science *287*, 664–666.
888 70. Yang, Z., Zhang, J., Jiang, D., Khatri, P., Solow-Cordero, D.E., Toesca, D.A.S., Koumenis,
889 C., Denko, N.C., Giaccia, A.J., Le, Q.-T., et al. (2018). A Human Genome-Wide RNAi Screen
890 Reveals Diverse Modulators that Mediate IRE1α-XBP1 Activation. Mol. Cancer Res. *16*,
891 745–753.
892 71. Ruland, J., and Hartjes, L. (2019). CARD-BCL-10-MALT1 signalling in protective and
893 pathological immunity. Nat. Rev. Immunol. *19*, 118–134.
894 72. Li, A., Song, N.-J., Riesenberg, B.P., and Li, Z. (2019). The Emerging Roles of Endoplasmic
895 Reticulum Stress in Balancing Immunity and Tolerance in Health and Diseases: Mechanisms
896 and Opportunities. Front. Immunol. *10*, 3154.
897 73. Reimold, A.M., Iwakoshi, N.N., Manis, J., Vallabhajosyula, P., Szomolanyi-Tsuda, E.,
898 Gravallese, E.M., Friend, D., Grusby, M.J., Alt, F., and Glimcher, L.H. (2001). Plasma cell
899 differentiation requires the transcription factor XBP-1. Nature *412*, 300–307.
900 74. Shaffer, A.L., Shapiro-Shelef, M., Iwakoshi, N.N., Lee, A.-H., Qian, S.-B., Zhao, H., Yu, X.,
901 Yang, L., Tan, B.K., Rosenwald, A., et al. (2004). XBP1, downstream of Blimp-1, expands
902 the secretory apparatus and other organelles, and increases protein synthesis in plasma cell
903 differentiation. Immunity *21*, 81–93.
904 75. Lee, A.-H., Heidtman, K., Hotamisligil, G.S., and Glimcher, L.H. (2011). Dual and opposing
905 roles of the unfolded protein response regulated by IRE1alpha and XBP1 in proinsulin
906 processing and insulin secretion. Proc. Natl. Acad. Sci. U. S. A. *108*, 8885–8890.
907 76. Batista, A., Rodvold, J.J., Xian, S., Searles, S.C., Lew, A., Iwawaki, T., Almanza, G., Waller,
908 T.C., Lin, J., Jepsen, K., et al. (2020). IRE1α regulates macrophage polarization, PD-L1
909 expression, and tumor survival. PLoS Biol. *18*, e3000687.
910 77. Pramanik, J., Chen, X., Kar, G., Henriksson, J., Gomes, T., Park, J.-E., Natarajan, K., Meyer,
911 K.B., Miao, Z., McKenzie, A.N.J., et al. (2018). Genome-wide analyses reveal the IRE1a-
912 XBP1 pathway promotes T helper cell differentiation by resolving secretory stress and
913 accelerating proliferation. Genome Med. *10*, 76.
914 78. Moretti, J., Roy, S., Bozec, D., Martinez, J., Chapman, J.R., Ueberheide, B., Lamming, D.W.,
915 Chen, Z.J., Horng, T., Yeretssian, G., et al. (2017). STING Senses Microbial Viability to
916 Orchestrate Stress-Mediated Autophagy of the Endoplasmic Reticulum. Cell *171*, 809-
917 823.e13.
918 79. Nunes-Hasler, P., and Demaurex, N. (2017). The ER phagosome connection in the era of
919 membrane contact sites. Biochim. Biophys. Acta Mol. Cell Res. *1864*, 1513–1524.
920 80. Sha, H., He, Y., Yang, L., and Qi, L. (2011). Stressed out about obesity: IRE1α-XBP1 in
921 metabolic disorders. Trends Endocrinol. Metab. *22*, 374–381.
922 81. Blasi, E., Radzioch, D., Merletti, L., and Varesio, L. (1989). Generation of macrophage cell
923 line from fresh bone marrow cells with a myc/raf recombinant retrovirus. Cancer Biochem.
924 Biophys. *10*, 303–317.
925 82. Hirota, M., Kitagaki, M., Itagaki, H., and Aiba, S. (2006). Quantitative measurement of spliced
926 XBP1 mRNA as an indicator of endoplasmic reticulum stress. J. Toxicol. Sci. *31*, 149–156.
927 83. Martin, M. (2011). Cutadapt removes adapter sequences from high-throughput sequencing
928 reads. EMBnet J. *17*, 10.
929 84. Bray, N.L., Pimentel, H., Melsted, P., and Pachter, L. (2016). Near-optimal probabilistic RNA-
930 seq quantification. Nat. Biotechnol. *34*, 525–527.
931 85. Love, M.I., Huber, W., and Anders, S. (2014). Moderated estimation of fold change and
932 dispersion for RNA-seq data with DESeq2. Genome Biol. *15*, 550.
933 86. Ost, K.S., O'Meara, T.R., Stephens, W.Z., Chiaro, T., Zhou, H., Penman, J., Bell, R.,
934 Catanzaro, J.R., Song, D., Singh, S., et al. (2021). Adaptive immunity induces mutualism
935 between commensal eukaryotes. Nature *596*, 114–118.